The Percellome method was developed for a large-scale toxicogenomics project [13] using the Affymetrix GeneChip system. It was intended to compile a very large-scale database of comprehensive gene expression profiles in response to various chemicals from a series of experiments conducted over an extended time period. However, the method also proved to be useful for small-scale platforms such as 96 well plate-based Q-PCRs as shown above, and probably for small-scale targeted microarrays. In both cases, highly inducible or highly transcribed genes are likely to be selected. Therefore, the expression profiles may differ significantly among samples such that profile-dependent normalization (e.g. global normalization) may not be applicable. In such cases, the profile-independent nature of the Percellome method provides a robust normalization.

To demonstrate the profile-independence of the Percellome method, we chose an extreme case – the uterotrophic response assay (cf. Figure 6). The treated uteri were composed of hypertrophic cells with abundant cytoplasm whereas the untreated uteri were composed of hypoplastic cells with scant cytoplasm. This indicates that the uteri of untreated ovariectomized mice were quiescent, and that a majority of the inducible genes were probably transcriptionally inactive. Therefore, the identification of most genes as being induced by 2-fold or greater is reasonable and expected. In most *in vivo* experiments, the gene profiles of the samples are much more similar. However, there is always a set of genes that is found to be "increased" when analyzed on a "per one cell" basis that are declared to be "decreased" by global type normalization, or vice versa. Such increase/decrease calls made by the global type normalization can differ according to the normalization parameters. In both cases, the Percellome method can inform the researcher how much the expression profiles are distorted by the treatment, such as in the case of the uterotrophic assay. We also note that *in vitro* experiments such as cell-based studies tend to generate data similar to that of uterotrophic experiment.

Conclusion

Percellome data can be compared directly among samples and among different studies, and between different platforms, without further normalization. Therefore, "percellome" normalization can serve as a standard method for exchanging and comparing data across different platforms and among different laboratories. We hope that the Percellome method will contribute to transcriptome-based studies by facilitating data exchanges among laboratories.

Methods

Animal experiments

C57BL/6 Cr Slc (SLC, Hamamatsu, Japan) mice maintained in a barrier system with a 12 h photoperiod were used in this study. For the liver transcriptome experiments, twelve week-old male mice were given a single dose of the test compound by oral gavage, and the liver was sampled at 2, 4, 8 and 24 h post-gavage. For the uterotrophic experiment, 6 week old female mice were ovariectomized 14 days prior to the 7 day repeated subcutaneous injection of a test compound [12]. Animals were euthanized by exsanguination under ether anesthesia and the target organs were excised into ice-cooled plastic dishes. Tissue blocks weighing 30 to 60 mg were placed in an RNase-free 2 ml plastic tube (Eppendorf GmbH., Germany) and soaked in RNAlater (Ambion Inc., TX) within 3 min of the beginning of anesthesia. Three animals per treatment group were used and individually subjected to transcriptome measurement.

Sample homogenate preparation

The tissue blocks soaked in RNAlater were kept overnight at 4°C or until use. RNAlater was replaced in the 2 ml plastic tube with 1.0 ml of RLT buffer (Qiagen GmbH., Germany), and the tissue was homogenized by adding a 5 mm diameter Zirconium bead (Funakoshi, Japan) and shaking with a MixerMill 300 (Qiagen GmbH., Germany) at a speed of 20 Hz for 5 min (only the outermost row of the shaker box was used).

Direct DNA quantitation

Three separate 10 μl aliquots were taken from each sample homogenate to another tube and mixed thoroughly. A final 10 μl aliquot therefrom was treated with DNAse-free RNase A (Nippon Gene Inc., Japan) for 30 min at 37°C, followed by Proteinase K (Roche Diagnostics GmbH., Germany) for 3 h at 55°C in 1.5 ml capped tubes. The aliquot was transferred to a 96-well black plate. PicoGreen fluorescent dye (Molecular Probes Inc., USA) was added to each well, shaken for 10 seconds four times and then incubated for 2 min at 30°C. The DNA concentration was measured using a 96 well fluorescence plate reader with excitation at 485 nm and emission at 538 nm. λ phage DNA (PicoGreen Kit, Molecular Probes Inc., USA) was used as standard. Measurement by this PicoGreen method and the standard phenol extraction method correlated well (coefficient of correlation = 0.97, data not shown). The smallest sample size for reproducible and reliable DNA quantitation is about 5,000 cells that corresponds to a 6.75 dpc mouse embryo.

The grade-dosed spike cocktail (GSC)

The following five *Bacillus subtilis* RNA sequences were selected from the gene list of Affymetrix GeneChip arrays (AFFX-ThrX-3_at, AFFX-LysX-3_at, AFFX-PheX-3_at, AFFX-DapX-3_at, and AFFX-TrpnX-3_at) present in the MG-U74v2, RG-U34, HG-U95, HG-U133, RAE230 and MOE430 arrays: thrC, thrB genes corresponding to nucleotides 248–2229 of X04603; lys gene for diami-

nopimelate decarboxylase corresponding to nucleotides 350–1345 of X17013; pheB, pheA genes corresponding to nucleotides 2017–3334 of M24537, dapB, jojF, jojG genes corresponding to nucleotides 1358–3197 of L38424; TrpE protein, TrpD protein, TrpC protein corresponding to nucleotides 1883–4400 of K01391. The corresponding cDNAs were purchased from ATCC, incorporated into expression vectors, amplified in *E. coli* and transcribed using the MEGAscript kit (Ambion Inc., TX). The mRNA was purified using a MACS mRNA isolation kit (Miltenyi Biotec GmbH., Germany). The concentrations of spike RNAs in the GSC were in threefold steps, from 777.6 pM for AFFX-ThrX-3_at, 259.4 pM for AFFX-LysX-3_at, 86.4 pM for AFFX-PheX-3_at, 28.8 pM for AFFX-DapX-3_at, to 9.6 pM for AFFX-TrpnX-3_at. In general, the ratio depends on the linear range of the measurement system and the available number of spikes.

Setting of the "spike factor" and addition of GSC to a sample homogenate according to its DNA concentration

The GSC was added to the sample homogenates in proportion to their DNA concentrations, assuming that all cells contain a fixed amount of genomic DNA (g/cell) across samples. The amount of GSC added to each sample G (l) was given as

$$G = C * v * f \quad (l),$$

where C is the DNA concentration (g/l), v(l) is the volume of homogenate further used for RNA extraction and f (l/g) is the "spike factor", which is an adjustment factor to ensure that the sample is properly spiked by the GSC (cf. Figure 3). Spike factors have been pre-determined for various organs/tissues to reflect differences in their total RNA/genomic DNA ratios (cf. Table 1). In this way, five spike mRNA signals can properly cover the linear dose-response range of the platform. In practice, for the Affymetrix GeneChips, the spike factor is set so that the five GSC spikes cover the range of "Present" calls given by the Affymetrix system, which corresponds to approximately 80 to 7000 in raw readouts given by the Affymetrix MAS5.0 software. A raw readout of 10 by the current Affymetrix GeneChip system corresponds to approximately one copy per cell in mouse liver (spike factor = 0.2), whereas in mouse thymus (spike factor = 0.01) it corresponds to approximately 0.05 copy per cell. For Q-PCR, the same spike factor corresponds to Ct values ranging approximately from 17 to 27, which is well within the linear range of Q-PCR (data not shown).

"Per cell" normalization (Percellome normalization)

Since murine haploid genomic DNA is made of 2.5×10^9 base pairs and one base pair is approximately 600 Daltons (Da), the haploid genomic DNA weighs 1.5×10^{12} Da, corresponding to

$d = 5 \times 10^{-12}$ (g DNA per diploid cell).

Therefore, the cell number per liter of the sample homogenate (N) is given as

$N = C/d$ (cells/l)

where C is the DNA concentration (g/l).

On the other hand, the copy numbers of GSC RNAs in the homogenate are given as follows:

if Sj (mole/l) (j = 1,2,3,4,5) is the mole concentration of one of the five spike RNAs in the GSC solution and G(l) is the amount of GSC added to each homogenate, the mole concentrations of the spike RNAs in the homogenate (CSj) are given as,

$CSj = Sj*C*f$ (mole/l).

The GSC RNAs in moles per cell (MSj) are given as

$MSj = CSj/N$

$= Sj*C*f/(C/d)$

$= Sj*f*d$ (mole/cell)

The copy numbers of the GSC RNAs per cell (NSj) are given as

$NSj = MSj*A$

$= Sj*f*d*A$ (copies per diploid cell)

where A is Avogadro's number.

As a result, the GSC spikes AFFX-TrpnX-3_at, AFFX-DapX-3_at, AFFX-PheX-3_at, AFFX-LysX-3_at and AFFX-ThrX-3_at correspond approximately to 5.8, 17.3, 52.0, 156.0 and 468.1 copies per cell (per diploid DNA template) for mouse liver sample homogenates, where the spike factor = 0.2. It is our observation that the RNA/DNA ratios are virtually constant across polyploid hepatocytes (data not shown).

For each Q-PCR plate or GeneChip, the coefficients, α, β, γ and δ of functions {1} or {2} are determined from the GSC values using the least-square method. The signal values or Ct values of all the other mRNAs measured are then converted to copy numbers per cell by {3} or {4}, i.e. the inverses of functions {1} or {2}.

Table 2: Primers for Q-PCR

Gene	Forward	Reverse
AFFX-TrpnX-3_at	TTCTCAGCGTAAAGCAATCCA	GCAAATCCTTTAGTGACCGAATACC
AFFX-DapX-3_at	TCAGCTAACGCTTCCAGACC	GGCCGACAGATTCTGATGACA
AFFX-PheX-3_at	GCCAATGATATGGCAGCTTCTAC	TGCGGCAGCATGACCATTA
AFFX-LysX-3_at	CCGCTTCATGCCACTGAATAC	CCGGTTCGATCCAAATTTCC
AFFX-ThrX-3_at	CCTGCATGAGGATGACGAGA	GGCATCGGCATATGGAAAC
Ahr_1450695_at	CAGAGACCACTGACGGATGAA	AGCCTCTCCGGTAGCAAACA
Cyp1a1_1422217_a_at	TGCTCTTGCCACCTGCTGA	GGAGCACCCTGTTTGTTTCTATG
Cyp1a2_1450715_at	CCTCACTGAATGGCTTCCAC	CGATGGCCGAGTTGTTATTG
Cyp1b1_1416612_at	GCCTCAGGTGTGTTTGATGGA	AGTACAGCCCTGGTGGGAATG
Cyp7a1_1422100_at	TTCTACATGCCCTTTGGATCAG	GGACACTTGGTGTGGCTCTC
Hspa1a_1452388_at	ACCATCGAGGAGGTGGATTAGA	AGGACTTGATTGCAGGACAAAC

The "LBM" ("liver-brain mix") standard sample

A pair of samples having dissimilar gene expression profiles was chosen to evaluate the linearity of the platform. The pairs chosen were brain and liver for mouse and rat, two distinct cancer cell lines for humans, and adult liver and embryo for *Xenopus laevis*. The sample pairs were processed as described above including addition of the GSC. Two final homogenates were then blended at ratios of 100:0, 75:25, 50:50, 25:75 and 0:100 (based on cell numbers) to make five samples. These five samples were measured by Q-PCR and/or GeneChips (MG-U74v2A, MEA430A, MEA430B, MG430 2.0 (shown in Figure 1), RAE230A, HG-U95A, HG-U133, and Xenopus array).

Quantitative-PCR

Duplicate homogenate samples were treated with DNaseI (amplification grade, Invitrogen Corp., Carlsbad, CA, USA) for 15 min at room temperature, followed by SuperScript II (Invitrogen) for 50 min at 42°C for reverse transcription. Quantitative real time PCR was performed with an ABI PRISM 7900 HT sequence detection system (Applied Biosystems, Foster City, CA, USA) using SYBR Premix Ex Taq (TAKARA BIO Inc., Japan), with initial denaturation at 95°C for 10 s followed by 45 cycles of 5 s at 95°C and 60 s at 60°C, and Ct values were obtained. Primers for the genes explored in this study were selected from sequences close to the areas of Affymetrix GeneChip probe sets as shown in Table 2.

Affymetrix GeneChip measurement

The sample homogenates with GSC added were processed by the Affymetrix Standard protocol. The GeneChips used were MG-U74v2A for the uterotrophic study and Mouse 430-2 for the TCDD study (singlet measurement). The efficiency of *in vitro* transcription (IVT) was monitored by comparing the values of 5' probe sets and 3' probe sets of the control RNAs (AFFX- probe sets) including the GSC (see Quality Control below). The dose-response linearity of the five GSC spikes was checked and samples showing saturation and/or high background were re-measured from either backup tissue samples, an aliquot of homogenate, or a hybridization solution, depending on the nature of the anomaly.

Quality control

Any external spiking method, including our Percellome method, is valid for high-quality RNA samples. Therefore, the quality of the sample RNA should be carefully monitored. In addition to a common checkup by RNA electrophoresis (including capillary electrophoresis if necessary), OD ratio, and cRNA yield, we monitor the performance of IVT (*in vitro* translation) or amplification. The 3' and 5' probe set data of the spiked-in RNAs and sample RNAs (actin, GAPD and other AFFX- probe sets) that are prepared in Affymetrix GeneChip are compared to monitor the extension of RNA by the IVT process. When both the spiked-in RNAs and the sample RNAs have similar levels of 5' and 3' signals respectively, it is judged that the IVT extension was normally performed. When both spiked-in and sample RNAs have significantly lower 5' signal than 3' signal, it is judged that the IVT extension was abnormal. When only the sample RNAs showed significantly lower 5' signal than 3' signal, it is judged that the IVT extension was normal but the sample RNAs were degraded. When only the spiked-in RNAs showed significantly lower 5' signal than 3' signal, it is judged that the IVT extension was normal but the spiked-in RNAs were degraded (although we have not encountered this situation). In addition, if the degraded sample was spiked-in by the non-degraded spike RNAs and measured by GeneChip, the position of spiked-in RNAs will be offset toward abnormally higher intensity. Together, this battery of checkups considerably increases the ability to detect abnormal events that will affect the reliability of the Percellome method. When any abnormality was found, each step of sample preparation was reevaluated to regain normal data for Percellome normalization.

The web site for GeneChip data

The GeneChip data are accessible at http://www.nihs.go.jp/tox/TTG_Archive.htm.

Authors' contributions

JK drafted the concept of the Percellome method, led the project at a practical level, and drafted the manuscript. KA developed the algorithm for the Percellome calculation and wrote the calculation/visualization programs. KI developed the laboratory protocols for the Percellome procedures to the level of SOP for technicians. NN developed the Percellome Q-PCR protocol and performed the measurements, and helped in analyzing the Percellome data. AO helped develop the algorithm. YK led the animal studies. TN provided advice and led the toxicogenomics project using the Percellome method, to be approved by the Ministry of Health, Labour and Welfare of Japan.

Additional material

Additional File 1

Excel spreadsheet file containing 15 Affymetrix Mouse 430–2 GeneChip raw data of five LBM samples in triplicate (cf. Figure 1). The column name LBM-100-0-X_Signal indicates the component percentages, i.e. 100% liver 0% brain, and X = 1,2,3 indicates the triplicates. The LBM-100-0-X_Detection column indicates P for present, A for absent and M for marginal calls by Affymetrix MAS 5.0 system.

Click here for file
[http://www.biomedcentral.com/content/supplementary/1471-2164-7-64-S1.zip]

Additional File 2

Excel spreadsheet file containing Percellome data of the same LBM samples, of which raw data is listed in Additional file 1 (cf. Figure 1).

Click here for file
[http://www.biomedcentral.com/content/supplementary/1471-2164-7-64-S2.zip]

Additional File 3

Excel spreadsheet file containing 2 Affymetrix MG-U74v2 raw data of a blank sample with the GSC (horizontal axis of Figure 2a) and blank with the five spike RNAs at a high dosage (vertical axis of Figure 2a).

Click here for file
[http://www.biomedcentral.com/content/supplementary/1471-2164-7-64-S3.zip]

Additional File 4

Excel spreadsheet file containing 2 Affymetrix MG-U74v2 raw data of a liver sample with GSC (horizontal axis of Figure 2b) and without GSC (vertical axis of Figure 2b).

Click here for file
[http://www.biomedcentral.com/content/supplementary/1471-2164-7-64-S4.zip]

Additional File 5

(first quarter of a data set consisting of 2 hr, 4 hr, 8 hr, and 24 hr data, divided because of the upload file size limitation)]: an Excel spreadsheet file containing 2 hr data (15 GeneChip data) of the total of 60 Affymetrix Mouse 430-2 GeneChip raw data of the TCDD study consisting of 20 different treatment groups in triplicate (cf. Figure 5). The column name DoseXXX-TimeYY-Z_Signal indicates the dosage and sampling time after TCDD administration in hours, e.g. XXX = 001 indicates 1 microgram/kg group, YY = 02 indicates two hours after administration, and Z = 1,2,3 indicates animal triplicate. The DoseXXX-TimeYY-Z_Detection column indicates P for present, A for absent and M for marginal calls by Affymetrix MAS 5.0 system.

Click here for file
[http://www.biomedcentral.com/content/supplementary/1471-2164-7-64-S5.zip]

Additional File 6

(second quarter of a data set consisting of 2 hr, 4 hr, 8 hr, and 24 hr data, divided because of the upload file size limitation)]: an Excel spreadsheet file containing 4 hr data (15 GeneChip data) of the total of 60 Affymetrix Mouse 430-2 GeneChip raw data of the TCDD study consisting of 20 different treatment groups in triplicate (cf. Figure 5). The column name DoseXXX-TimeYY-Z_Signal indicates the dosage and sampling time after TCDD administration in hours, e.g. XXX = 001 indicates 1 microgram/kg group, YY = 02 indicates two hours after administration, and Z = 1,2,3 indicates animal triplicate. The DoseXXX-TimeYY-Z_Detection column indicates P for present, A for absent and M for marginal calls by Affymetrix MAS 5.0 system.

Click here for file
[http://www.biomedcentral.com/content/supplementary/1471-2164-7-64-S6.zip]

Additional File 7

(third quarter of a data set consisting of 2 hr, 4 hr, 8 hr, and 24 hr data, divided because of the upload file size limitation)]: an Excel spreadsheet file containing 8 hr data (15 GeneChip data) of the total of 60 Affymetrix Mouse 430-2 GeneChip raw data of the TCDD study consisting of 20 different treatment groups in triplicate (cf. Figure 5). The column name DoseXXX-TimeYY-Z_Signal indicates the dosage and sampling time after TCDD administration in hours, e.g. XXX = 001 indicates 1 microgram/kg group, YY = 02 indicates two hours after administration, and Z = 1,2,3 indicates animal triplicate. The DoseXXX-TimeYY-Z_Detection column indicates P for present, A for absent and M for marginal calls by Affymetrix MAS 5.0 system.

Click here for file
[http://www.biomedcentral.com/content/supplementary/1471-2164-7-64-S7.zip]

Additional File 8

(last quarter of a data set consisting of 2 hr, 4 hr, 8 hr, and 24 hr data, divided because of the upload file size limitation)]: an Excel spreadsheet file containing 24 hr data (15 GeneChip data) of the total of 60 Affymetrix Mouse 430-2 GeneChip raw data of the TCDD study consisting of 20 different treatment groups in triplicate (cf. Figure 5). The column name DoseXXX-TimeYY-Z_Signal indicates the dosage and sampling time after TCDD administration in hours, e.g. XXX = 001 indicates 1 microgram/kg group, YY = 02 indicates two hours after administration, and Z = 1,2,3 indicates animal triplicate. The DoseXXX-TimeYY-Z_Detection column indicates P for present, A for absent and M for marginal calls by Affymetrix MAS 5.0 system.

Click here for file
[http://www.biomedcentral.com/content/supplementary/1471-2164-7-64-S8.zip]

Additional File 9

(first quarter of a data set consisting of 2 hr, 4 hr, 8 hr, and 24 hr data, divided because of the upload file size limitation)]: an Excel spreadsheet file containing 2 hr Percellome data (15 sample data) of the 60 samples of the TCDD study (cf. Figure 5), of which corresponding raw data is listed in Additional file 5.
Click here for file
[http://www.biomedcentral.com/content/supplementary/1471-2164-7-64-S9.zip]

Additional File 10

(second quarter of a data set consisting of 2 hr, 4 hr, 8 hr, and 24 hr data, divided because of the upload file size limitation)]: an Excel spreadsheet file containing 4 hr Percellome data (15 sample data) of the 60 samples of the TCDD study (cf. Figure 5), of which corresponding raw data is listed in Additional file 6.
Click here for file
[http://www.biomedcentral.com/content/supplementary/1471-2164-7-64-S10.zip]

Additional File 11

(third quarter of a data set consisting of 2 hr, 4 hr, 8 hr, and 24 hr data, divided because of the upload file size limitation)]: an Excel spreadsheet file containing 8 hr Percellome data (15 sample data) of the 60 samples of the TCDD study (cf. Figure 5), of which corresponding raw data is listed in Additional file 7.
Click here for file
[http://www.biomedcentral.com/content/supplementary/1471-2164-7-64-S11.zip]

Additional File 12

(last quarter of a data set consisting of 2 hr, 4 hr, 8 hr, and 24 hr data, divided because of the upload file size limitation)]: an Excel spreadsheet file containing 24 hr Percellome data (15 sample data) of the 60 samples of the TCDD study (cf. Figure 5), of which corresponding raw data is listed in Additional file 8.
Click here for file
[http://www.biomedcentral.com/content/supplementary/1471-2164-7-64-S12.zip]

Additional File 13

Excel spreadsheet file containing 15 Affymetrix MG-U74v2 A GeneChip raw data of the uterotrophic response study (cf. Figure 6). The column name X-Y_Signal indicates the treatment (V = vehicle, Low = low dose, etc) and animal triplicate (Y = 1,2,3). The X-Y_Detection column indicates P for present, A for absent and M for marginal calls by Affymetrix MAS 5.0 system.
Click here for file
[http://www.biomedcentral.com/content/supplementary/1471-2164-7-64-S13.zip]

Additional File 14

Excel spreadsheet file containing Percellome data of the same 15 samples of the uterotrophic response study (cf. Figure 6), of which raw data is listed in Additional file 13.
Click here for file
[http://www.biomedcentral.com/content/supplementary/1471-2164-7-64-S14.zip]

Acknowledgements

The authors thank Tomoko Ando, Noriko Moriyama, Yuko Kondo, Yuko Nakamura, Maki Abe, Nae Matsuda, Kenta Yoshiki, Ayako Imai, Koichi Morita, Hisako Aihara and Chiyuri Aoyagi for technical support, and Dr. Bruce Blumberg and Dr. Thomas Knudson for critical reading of the manuscript. This study was supported by Health Sciences Research Grants H13-Seikatsu-012, H13-Seikatsu-013, H14-Toxico-001 and H15-Kagaku-002 from the Ministry of Health, Labour and Welfare, Japan.

References

1. Holstege FC, Jennings EG, Wyrick JJ, Lee TI, Hengartner CJ, Green MR, Golub TR, Lander ES, Young RA: **Dissecting the regulatory circuitry of a eukaryotic genome.** *Cell* 1998, **95**:717-728.
2. Hill AA, Brown EL, Whitley MZ, Tucker-Kellogg G, Hunter CP, Slonim DK: **Evaluation of normalization procedures for oligonucleotide array data based on spiked cRNA controls.** *Genome Biol* 2001, **2**:. RESEARCH0055
3. Lee PD, Sladek R, Greenwood CM, Hudson TJ: **Control genes and variability: absence of ubiquitous reference transcripts in diverse mammalian expression studies.** *Genome Res* 2002, **12**:292-297.
4. van de Peppel J, Kemmeren P, van Bakel H, Radonjic M, van Leenen D, Holstege FC: **Monitoring global messenger RNA changes in externally controlled microarray experiments.** *EMBO Rep* 2003, **4**:387-393.
5. Yang YH, Dudoit S, Luu P, Lin DM, Peng W, Ngai J, Speed TP: **Normalization for cDNA microarray data: a robust composite method addressing single and multiple slide systematic variation.** *Nucleic Acids Res* 2002, **30**:e15.
6. Hekstra D, Taussig AR, Magnasco M, Naef F: **Absolute mRNA concentrations from sequence-specific calibration of oligonucleotide arrays.** *Nucleic Acids Res* 2003, **31**:1962-1968.
7. Sterrenburg E, Turk R, Boer JM, van Ommen GB, den Dunnen JT: **A common reference for cDNA microarray hybridizations.** *Nucleic Acids Res* 2002, **30**:e116.
8. Dudley AM, Aach J, Steffen MA, Church GM: **Measuring absolute expression with microarrays with a calibrated reference sample and an extended signal intensity range.** *Proc Natl Acad Sci USA* 2002, **99**:7554-7559.
9. Talaat AM, Howard ST, Hale W, Lyons R, Gamer H, Johnston ST: **Genomic DNA standards for gene expression profiling in Mycobacterium tuberculosis.** *Nucleic Acids Res* 2002, **30**:e104.
10. Bolstad BM, Irizarry RA, Astrand M, Speed TP: **A comparison of normalization methods for high density oligonucleotide array data based on variance and bias.** *Bioinformatics* 2003, **19**:185-193.
11. Lockhart DJ, Dong H, Byrne MC, Follettie MT, Gallo MV, Chee MS, Mittmann M, Wang C, Kobayashi M, Horton H, Brown EL: **Expression monitoring by hybridization to high-density oligonucleotide arrays.** *Nat-Biotechnol* 1996, **14**:1675-1680.
12. Kanno J, Onyon L, Peddada S, Ashby J, Jacob E, Owens W: **The OECD program to validate the rat uterotrophic bioassay. Phase 2: dose-response studies.** *Environ Health Perspect* 2003, **111**:1530-1549.
13. Kanno J: **Reverse toxicology as a future predictive toxicology.** In *Toxicogenomics* Edited by: Inoue T, Pennie ED. Tokyo, Springer-Verlag; 2002:213-218.

PNAS
Proceedings of the National Academy of Sciences of the United States of America www.pnas.org

From the Cover: Premature ovarian failure in androgen receptor-deficient mice

Hiroko Shiina, Takahiro Matsumoto, Takashi Sato, Katsuhide Igarashi, Junko Miyamoto, Sayuri Takemasa, Matomo Sakari, Ichiro Takada, Takashi Nakamura, Daniel Metzger, Pierre Chambon, Jun Kanno, Hiroyuki Yoshikawa, and Shigeaki Kato

PNAS 2006;103;224-229; originally published online Dec 22, 2005;
doi:10.1073/pnas.0506736102

Premature ovarian failure in androgen receptor-deficient mice

Hiroko Shiina*†‡, Takahiro Matsumoto*‡§, Takashi Sato*, Katsuhide Igarashi¶, Junko Miyamoto*, Sayuri Takemasa*, Matomo Sakari*§, Ichiro Takada*, Takashi Nakamura*§, Daniel Metzger‖, Pierre Chambon‖, Jun Kanno¶, Hiroyuki Yoshikawa†, and Shigeaki Kato*§**

*Institute of Molecular and Cellular Biosciences, University of Tokyo, 1-1-1 Yayoi, Bunkyo-ku, Tokyo 113-0032, Japan; §Exploratory Research for Advanced Technology, Japan Science and Technology, 4-1-8 Honcho, Kawaguchi, Saitama 332-0012, Japan; †Department of Obstetrics and Gynecology, Institute of Clinical Medicine, University of Tsukuba, 1-1-1 Tennoudai, Tsukuba, Ibaraki 305-8575, Japan; ¶Division of Cellular and Molecular Toxicology, National Institute of Health Sciences, 1-18-1 Kamiyoga, Setagaya-ku, Tokyo 158-8501, Japan; and ‖Institut de Genetique et de Biologie Moleculaire et Cellulaire, Centre National de la Recherche Scientifique, Institut National de la Santé et de la Recherche Médicale, Universite Louis Pasteur, College de France, 67404 Illkirch, Strasbourg, France

Edited by Bert W. O'Malley, Baylor College of Medicine, Houston, TX, and approved November 10, 2005 (received for review August 5, 2005)

Premature ovarian failure (POF) syndrome, an early decline of ovarian function in women, is frequently associated with X chromosome abnormalities ranging from various Xq deletions to complete loss of one of the X chromosomes. However, the genetic locus responsible for the POF remains unknown, and no candidate gene has been identified. Using the Cre/LoxP system, we have disrupted the mouse X chromosome androgen receptor (*Ar*) gene. Female $AR^{-/-}$ mice appeared normal but developed the POF phenotype with aberrant ovarian gene expression. Eight-week-old female $AR^{-/-}$ mice are fertile, but they have lower follicle numbers and impaired mammary development, and they produce only half of the normal number of pups per litter. Forty-week-old $AR^{-/-}$ mice are infertile because of complete loss of follicles. Genome-wide microarray analysis of mRNA from $AR^{-/-}$ ovaries revealed that a number of major regulators of folliculogenesis were under transcriptional control by AR. Our findings suggest that AR function is required for normal female reproduction, particularly folliculogenesis, and that AR is a potential therapeutic target in POF syndrome.

male hormone | nuclear receptor | female physiology | folliculogenesis | kit ligand

Premature ovarian failure (POF) is defined as an early decline of ovarian function after seemingly normal folliculogenesis (1). Genetic causes of POF have been frequently associated with X chromosome abnormalities (1, 2). Complete loss of one of the X chromosomes, as in Turner syndrome, and various Xq deletions are commonly identified as a cause of POF. However, responsible X-linked genes and their downstream targets have not been identified so far.

The androgen receptor (*Ar*) gene, which is the only sex hormone receptor gene on the X chromosome, is well known to be essential not only for the male reproductive system, but also for male physiology. In contrast, androgens are considered as male hormones; therefore, little is known about androgens' actions in female physiology, although AR expression in growing follicles has been described (3). However, because excessive androgen production in polycystic ovary syndrome causes infertility with abnormal menstrual cycles (4, 5), it is possible that AR-mediated androgen signaling also plays an important physiological role in the female reproductive system. Recently, using Cre/LoxP system, we generated an AR-null mutant mouse line (6) and demonstrated that inactivation of AR resulted in arrest of testicular development and spermatogenesis, impaired brain masculinization, high-turnover osteopenia, and late onset of obesity in males (7–9). At the same time, no overt physical or growth abnormalities were observed in female $AR^{-/-}$ mice. Therefore, to further examine potential role of AR in female physiology, we characterized female reproductive system in $AR^{-/-}$ females. Herein we show that female $AR^{-/-}$ mice develop the POF phenotype. At 3 weeks of age, $AR^{-/-}$ females had apparently normal ovaries with numbers of follicles similar to those in the wild-type females. However, thereafter the number of healthy follicles in the $AR^{-/-}$ ovary gradually declined, with a marked increase of atretic follicles, and by 40 weeks $AR^{-/-}$ mice became infertile, with no follicle detectable in the ovary. Reflecting this age-dependent progression in ovarian abnormality, several genes known to be involved in the oocyte–granulosa cell regulatory loop were identified by microarray analysis as AR downstream target genes. These findings clearly demonstrate that AR-mediated androgen signaling is indispensable for the maintenance of folliculogenesis and implicate impaired androgen signaling as a potential cause of the POF syndrome.

Materials and Methods

Generation of AR Knockout Mice. *AR* genomic clones were isolated from a TT2 embryonic stem cell genomic library by using human *AR* A/B domain cDNA as a probe (6). The targeting vector consisted of a 7.6-kb 5′ region containing exon 1, a 1.3-kb 3′ homologous region, a single loxP site, and a neo cassette with two loxP sites (10). Targeted clones (FB-18 and FC-61) were aggregated with single eight-cell embryos from CD-1 mice (11, 12). Floxed *AR* mice (C57BL/6) were then crossed with CMV-Cre transgenic mice (6). The two lines exhibited the same phenotypic abnormalities. The chromosomal sex of each pup was determined by genomic PCR amplification of the Y chromosome *Sry* gene (13).

Western Blot Analysis. To detect AR protein expression, ovarian cell lysates were separated by SDS/PAGE and transferred onto nitrocellulose membranes (14). Membranes were probed with polyclonal AR antibodies (N-20; Santa Cruz Biotechnology), and blots were visualized by using peroxidase-conjugated second antibody and an ECL detection kit (Amersham Pharmacia Biosciences).

Morphologic Classification of Growing Follicles. Sections were taken at intervals of 30 μm, and 6-μm paraffin-embedded sections were mounted on slides. Routine hematoxylin and eosin staining was performed for histologic examination by light microscopy. Follicle numbers in 12 sections per ovary were evaluated as primary follicles (oocyte surrounded by a single layer of cuboidal granulosa cells), preantral follicles (oocyte surrounded by two or

Conflict of interest statement: No conflicts declared.

This paper was submitted directly (Track II) to the PNAS office.

Abbreviations: AR, androgen receptor; DHT, 5α-dihydrotestosterone; POF, premature ovarian failure.

†H.S. and T.M. contributed equally to this work.

**To whom correspondence should be addressed. E-mail: uskato@mail.ecc.u-tokyo.ac.jp.

www.pnas.org/cgi/doi/10.1073/pnas.0506736102

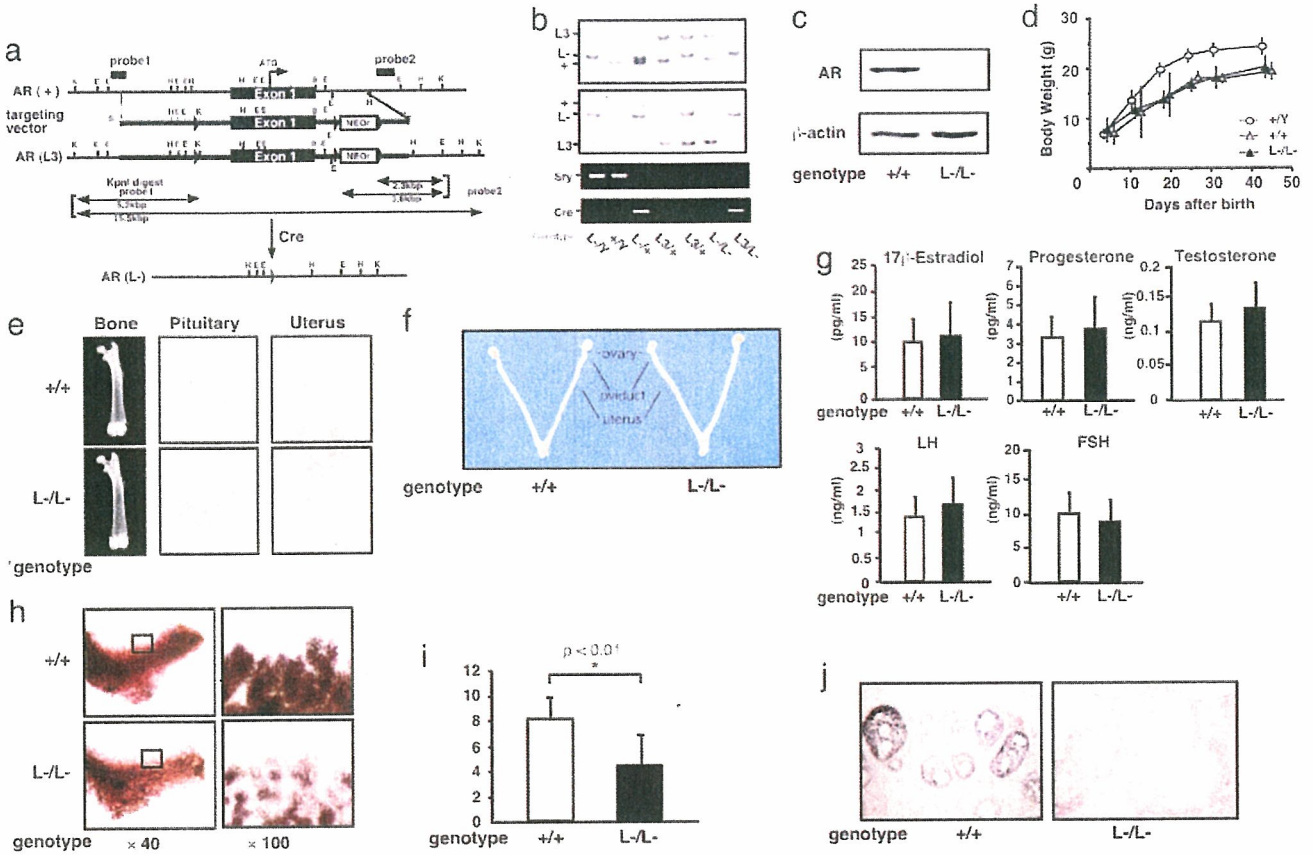

Fig. 1. Phenotypic characterization of AR knockout female mice. (*a*) Diagram of the wild-type *Ar* genomic locus (+), floxed *AR* L3 allele (L3), and *AR* allele (L-) obtained after Cre-mediated excision of exon 1. K, KpnI; E, EcoRI; H, HindIII; B, BamHI. LoxP sites are indicated by arrowheads. The targeting vector consisted of a 7.6-kb 5′ homologous region containing exon 1, a 1.3-kb 3′ homologous region, a single loxP site, and the neo cassette with two loxP sites. (*b*) Detection of the Y chromosome-specific *Sry* gene in $AR^{-/Y}$ mice by PCR. (*c*) Absence of AR protein in $AR^{-/-}$ mice ovaries by Western blot analysis using a specific C-terminal antibody. (*d*) Normal weight gain in $AR^{-/-}$ females. (*e*) Histology of pituitary, uterus, and bone tissues in $AR^{+/+}$ and $AR^{-/-}$ females at 8 weeks of age. (*f*) Female reproductive organs were macroscopically normal in $AR^{-/-}$ mice. (*g*) Serum hormone levels at the proestrus stage in $AR^{-/-}$ mice were not significantly altered. Serum 17β-estradiol, progesterone, testosterone, luteinizing hormone (LH), and follicle-stimulating hormone (FSH) levels in $AR^{+/+}$ ($n = 13$) and $AR^{-/-}$ ($n = 10$) females at 8–10 weeks of age are shown. (*h*) Lobuloalveolar development is impaired in $AR^{-/-}$ mammary glands. Whole mount of inguinal mammary glands (*Left*) and its higher magnification (*Right*) were prepared on day 3 of lactation. (*i*) Average number of pups per litter is markedly reduced in $AR^{-/-}$ mice at 8 weeks of age. Data are shown as mean ± SEM and analyzed by using Student's *t* test. (*j*) AR immunocytochemistry in $AR^{+/+}$ and $AR^{-/-}$ ovaries. Sections were counterstained with eosin.

more layers of granulosa cells with no antrum), or antral follicles (antrum within the granulosa cell layers enclosing the oocyte). Follicles were determined to be atretic if they displayed two or more of the following criteria within a single cross section: more than two pyknotic nuclei, granulosa cells within the antral cavity, granulosa cells pulling away from the basement membrane, or uneven granulosa cell layers (15).

Immunohistochemistry. Sections were subjected to a microwave antigen retrieval technique by boiling in 10 mM citrate buffer (pH 6.0) in a microwave oven for 30 min (16). The cooled sections were incubated in 1% H_2O_2 for 30 min to quench endogenous peroxidase and then incubated with 1% Triton X-100 in PBS for 10 min. To block nonspecific antibody binding, sections were incubated in normal goat serum for 1 h at 4°C. Sections were then incubated with anti-AR (1:100) or anti-cleaved caspase-3 (1:100) in 3% BSA overnight at 4°C. Negative controls were incubated in 3% BSA without primary antibody. The ABC method was used to visualize signals according to the manufacturer's instructions. Sections were incubated in biotinylated goat anti-rabbit IgG (1:200 dilution) for 2 h at room temperature, washed with PBS, and incubated in avidin–biotin–horseradish peroxidase for 1 h. After thorough washing in PBS, sections were developed with 3,3′-diaminobendizine tetrahydrochloride substrate, slightly counterstained with eosin, dehydrated through an ethanol series and xylene, and mounted.

Estrus Cycles and Fertility Test. To determine the stage of the estrus cycle (proestrus, estrus, and diestrus), vaginal smears were taken every morning and stained with Giemsa solution. For evaluation of female fertility for 15 weeks, an 8- or 24-week-old wild-type or $AR^{-/-}$ female was mated with a wild-type fertile male, replaced every 2 weeks with the other fertile male. Cages were monitored daily and for an additional 23 days, and the presence of seminal plugs and number of litters were recorded.

RNA Extraction and Quantitative Competitive RT-PCR. Total ovarian RNA was extracted by using TRIzol (Invitrogen) (16). Oligo-dT-primed cDNA was synthesized from 1 μg of ovarian RNA by using SuperScript reverse transcriptase (Gibco BRL, Gaithersburg, MD) in a 20-μl reaction volume, 1 μl of which was then diluted serially (2- to 128-fold) and used to PCR-amplify an internal control gene, *cycA*, to allow concentration estimation.

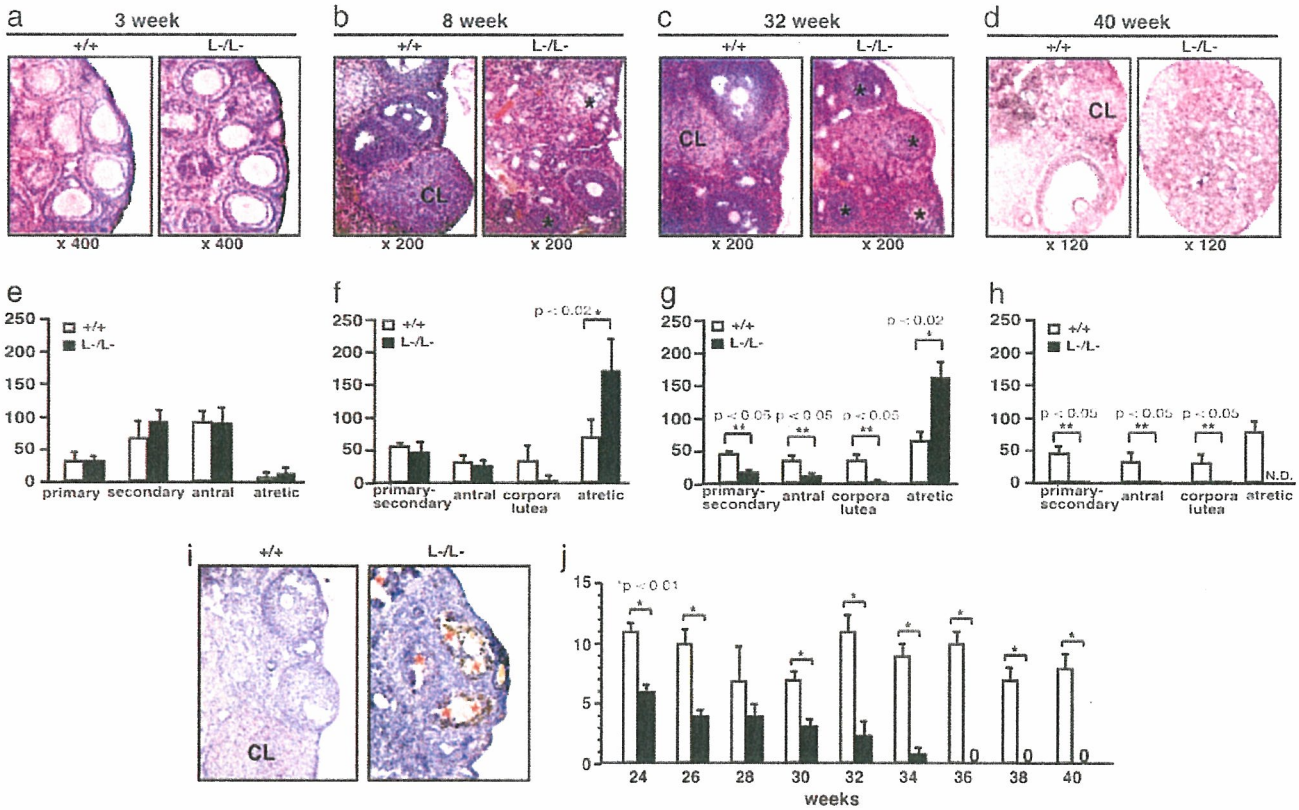

Fig. 2. POF in $AR^{-/-}$ female mice. (*a–d*) Histology of $AR^{+/+}$ and $AR^{-/-}$ ovaries at 3 weeks, 8 weeks, 32 weeks, and 40 weeks of age. All sections were stained with hematoxylin and eosin. An asterisk marks the atretic follicle. CL, corpus luteum. (*e–h*) Relative follicle counts at 3 weeks (*e*), 8 weeks (*f*), 32 weeks (*g*), and 40 weeks (*h*) of age. Numbers represent total counts of every fifth section from serially sectioned ovaries ($n = 4$ animals per genotype). (*i*) Immunohistochemical study for activated, cleaved caspase-3 revealed increased positive cells (apoptotic cells) in $AR^{-/-}$ ovaries. Sections were counterstained with hematoxylin. An asterisk marks the caspase-3-positive cell. CL, corpus luteum. (*j*) Age-dependent reduction in the number of pups per litter in $AR^{-/-}$ female mice. A continuous breeding assay was started at 24 weeks of age ($n = 6–10$ animals per genotype). For all panels, data are shown as mean ± SEM and were analyzed by using Student's *t* test.

Primers were designed from cDNA sequences of *Kitl* (M57647; nucleotides 1099–1751), Gdf9 (NM008110; nucleotides 720-1532), *Bmp15* (NM009757; nucleotides 146–973), *Ers2* (NM010157; nucleotides 1139–1921), *Pgr* (NM008829; nucleotides 1587–2425), *Cyp11a1* (NM019779; nucleotides 761-1697), *Cyp17a1* (M64863; nucleotides 522–932), *Cyp19* (D00659; nucleotides 699-1049), *Fshr* (AF095642; nucleotides 625-1427), *Lhr* (M81310; nucleotides 592-1331), *Ptgs2* (AF338730; nucleotides 3–605), and *Ccnd2* (NM009829; nucleotides 150-1065) and chosen from different exons to avoid amplification from genomic DNA.

GeneChip Analysis. Ovaries were isolated and stabilized in RNA-*later* RNA Stabilization Reagent (Ambion, Austin, TX) before RNA purification (17). Total RNA was purified by using an RNeasy mini kit (Qiagen, Valencia, CA) according to the manufacturer's instructions. First-strand cDNA was synthesized from 5 μg of RNA by using 200 units of SuperScript II reverse transcriptase (Invitrogen, Carlsbad, CA), 100 pmol T7-$(dT)_{24}$ primer [5′-GGCCAGTGAATTGTAATACGACTCAC-TATAGGGAGGCGG-$(dT)_{24}$-3′], 1× first-strand buffer, and 0.5 mM dNTPs at 42°C for 1 h. Second-strand synthesis was performed by incubating first-strand cDNA with 10 units of *Escherichia coli* ligase (Invitrogen), 40 units of DNA polymerase I (Invitrogen), 2 units of RNase H (Invitrogen), 1× reaction buffer, and 0.2 mM dNTPs at 16°C for 2 h, followed by 10 units of T4 DNA polymerase (Invitrogen) and incubation for another 5 min at 16°C. Double-stranded cDNA was purified by using GeneChip Sample Cleanup Module (Affymetrix, Santa Clara, CA) according to the manufacturer's instructions and labeled by *in vitro* transcription by using a BioArray HighYield RNA transcript labeling kit (Enzo Diagnostics, Farmingdale, NY). Briefly, dsDNA was mixed with 1× HY reaction buffer, 1× biotin-labeled ribonucleotides (NTPs with Bio-UTP and Bio-CTP), 1× DTT, 1× RNase inhibitor mix, and 1× T7 RNA polymerase and incubated at 37°C for 4 h. Labeled cRNA was then purified by using GeneChip Sample Cleanup Module and fragmented in 1× fragmentation buffer at 94°C for 35 min. For hybridization to the GeneChip Mouse Expression Array 430A or 430B or Mouse Genome 430 2.0 Array (Affymetrix), 15 μg of fragmented cRNA probe was incubated with 50 pM control oligonucleotide B2, 1× eukaryotic hybridization control, 0.1 mg/ml herring sperm DNA, 0.5 mg/ml acetylated BSA, and 1× hybridization buffer in a 45°C rotisserie oven for 16 h. Washing and staining were performed by using a GeneChip Fluidic Station (Affymetrix) according to the manufacturer's protocol. Phycoerythrin-stained arrays were scanned as digital image files and analyzed with GENECHIP OPERATING SOFTWARE (Affymetrix) (17).

Luciferase Assay. The *Kitl* promoter region (−2866 to −1 bp) was inserted into the pGL3-basic vector (Promega) for assay using the Luciferase Assay System (Promega) (14, 16). Cells at 40–50% confluence were transfected with a reference pRL-CMV

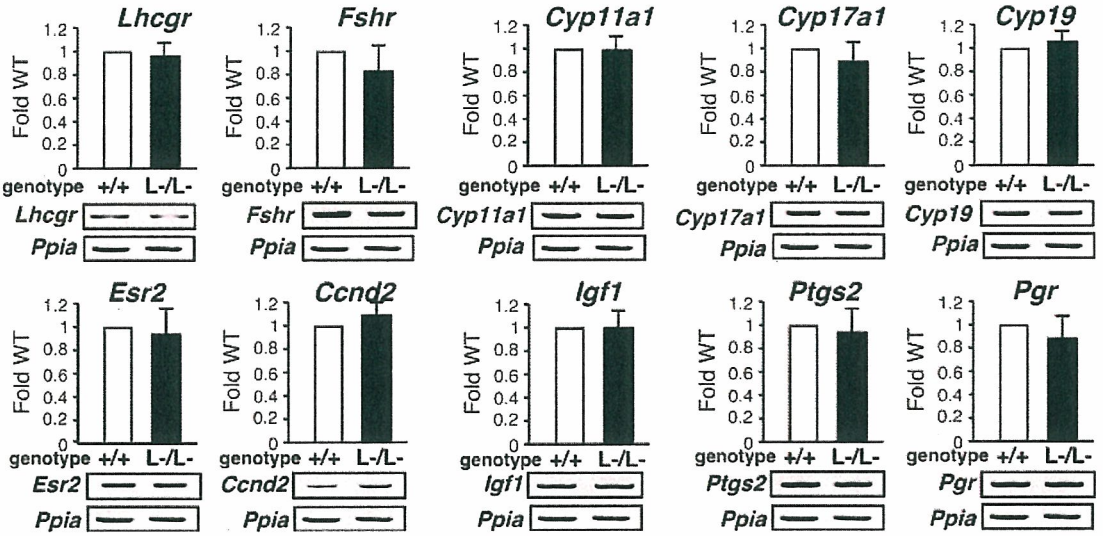

Fig. 3. No significant alterations in mRNA levels of several major regulators in folliculogenesis. Shown is semiquantitative RT-PCR of LH receptor (*Lhr*), FSH receptor (*Fshr*), p450 side chain cleavage enzyme (*Cyp11a1*), 17-α-hydroxylase (*Cyp17a1*), Aromatase (*Cyp19*), estrogen receptor-β (*Esr2*), cyclin D2 (*Ccnd2*), insulin-like growth factor 1 (*Igf1*), cyclooxygenase 2 (*Ptgs2*), or progesterone receptor (*Pgr*) gene expression in $AR^{+/+}$ and $AR^{-/-}$ ovaries. Results shown were representative (using one ovary per genotype in each experiment) of five independent experiments.

plasmid (Promega) using Lipofectamine reagent (GIBCO/BRL, Grand Island, NY) to normalize transfection. Results shown are representative of five independent experiments.

Results and Discussion

Subfertility of $AR^{-/-}$ Female Mice at 8 Weeks of Age. The *Ar* gene located on the X chromosome was disrupted in mice by using the Cre/Lox P system (6) (Fig. 1 *a–c*). Female $AR^{-/-}$ mice showed normal growth compared with the wild-type littermates (Fig. 1*d*), with no detectable bone loss (Fig. 1*e*) or obesity common for male $AR^{-/Y}$ mice (8, 9). Young (8-week-old) $AR^{-/-}$ females appeared indistinguishable from the wild-type littermates, displayed normal sexual behavior (7), and produced the first offspring of normal body size at the expected age. Macroscopic appearance of their reproductive organs, including uteri, oviducts, and ovaries, also appeared normal (Fig. 1*f*). Histological analysis showed no significant abnormality in the uterus or pituitary (Fig. 1*e*), whereas mammary ductal branching and elongation were substantially reduced, as revealed by whole-mount analysis (Fig. 1*h*). Serum levels of 17β-estradiol, progesterone, testosterone, luteinizing hormone, and follicle-stimulating hormone were also within normal range in 8-week-old mutant females at the proestrus stage (Fig. 1*g*), suggesting that the two-cell two-gonadotrophin system in female reproductive and endocrine organs (18) was intact in $AR^{-/-}$ mice at 8 weeks of age. The most obvious early sign of abnormal reproductive function in the $AR^{-/-}$ females was that their average numbers of pups per litter were only about half of those of the wild-type littermates, ($AR^{+/+}$, 8.3 ± 0.4 pups per litter; $AR^{-/-}$, 4.5 ± 0.5 pups per litter) (Fig. 1*i*).

$AR^{-/-}$ Female Mice Developed POF Phenotypes. Histological analysis of 8-week-old $AR^{-/-}$ ovaries clearly showed that numbers of atretic follicles were significantly increased, with decreased numbers of corpora lutea (Fig. 2 *b* and *f*). This finding suggests that the reduced pup numbers were due to impaired folliculogenesis in AR-deficient ovaries. Indeed, AR protein expression was readily detectable in the wild-type 8-week-old ovaries (Fig. 1*j*), with AR expressed at the highest levels in growing follicle granulosa cells at all developmental stages and at relatively low levels in corpora lutea. Thus, AR appears to play a regulatory role in granulosa cells during their maturation to the luteal phase.

To investigate this possibility, we examined the ovarian phenotype of female $AR^{-/-}$ mice at different ages. At 3 weeks, ovaries contain various stages of follicles, including primary, secondary, and antral follicles in wild-type animals (Fig. 2*a*) (19). In $AR^{-/-}$ ovaries at 3 weeks of age, the folliculogenesis appeared to be unaltered, with normal numbers and localization of primary and secondary follicles (Fig. 2 *a* and *e*). However, degenerated folliculogenesis became evident with further aging. Although follicles and corpora lutea at all developmental stages were still present, corpora lutea numbers were clearly reduced in 8-week-old $AR^{-/-}$ mutants (Fig. 2 *b* and *f*), similar to that observed in another mouse line (20). Expected apoptosis was seen in atretic follicles by activated caspase-3 immunohistochemistry assays (Fig. 2*i*). But, by 32 weeks of age, defects in folliculogenesis in $AR^{-/-}$ ovaries became profound, with fewer follicles observed and increased atretic follicles (Fig. 2 *c* and *g*), and >40% (5 of 12 mice) of the $AR^{-/-}$ females were already infertile. By 40 weeks, all $AR^{-/-}$ females became infertile, with no follicles remaining (Fig. 2 *d* and *h*); at the same age, $AR^{+/+}$ females were fertile and had normal follicle numbers. Consistent with progressive deficiency in folliculogenesis, the pup number per litter steadily decreased in aging $AR^{-/-}$ females (Fig. 2*i*). These data indicate that AR plays an important physiological role at the preluteal phase of folliculogenesis.

Alteration in Gene Expressions of Several Major Regulators Involved in the Oocyte–Granulosa Cell Regulatory Loop. To explore the molecular basis underlying the impaired folliculogenesis in $AR^{-/-}$ ovaries, we analyzed expression of several major known regulators and markers of folliculogenesis (21–23). Surprisingly, no significant alterations in mRNA levels of LH receptor (*Lhr*), FSH receptor (*Fshr*), p450 side chain cleavage enzyme (*Cyp11a1*), 17-α-hydroxylase (*Cyp17a1*), aromatase (*Cyp19*), estrogen receptor-β (*Esr2*), cyclin D2 (*Ccnd2*), or insulin-like growth factor 1 (*Igf1*) of 8-week-old $AR^{-/-}$ ovaries at the proestrus stage, and further cyclooxygenase 2 (*Ptgs2*) or progesterone receptor (*Pgr*) at the estrus stage, were detected by

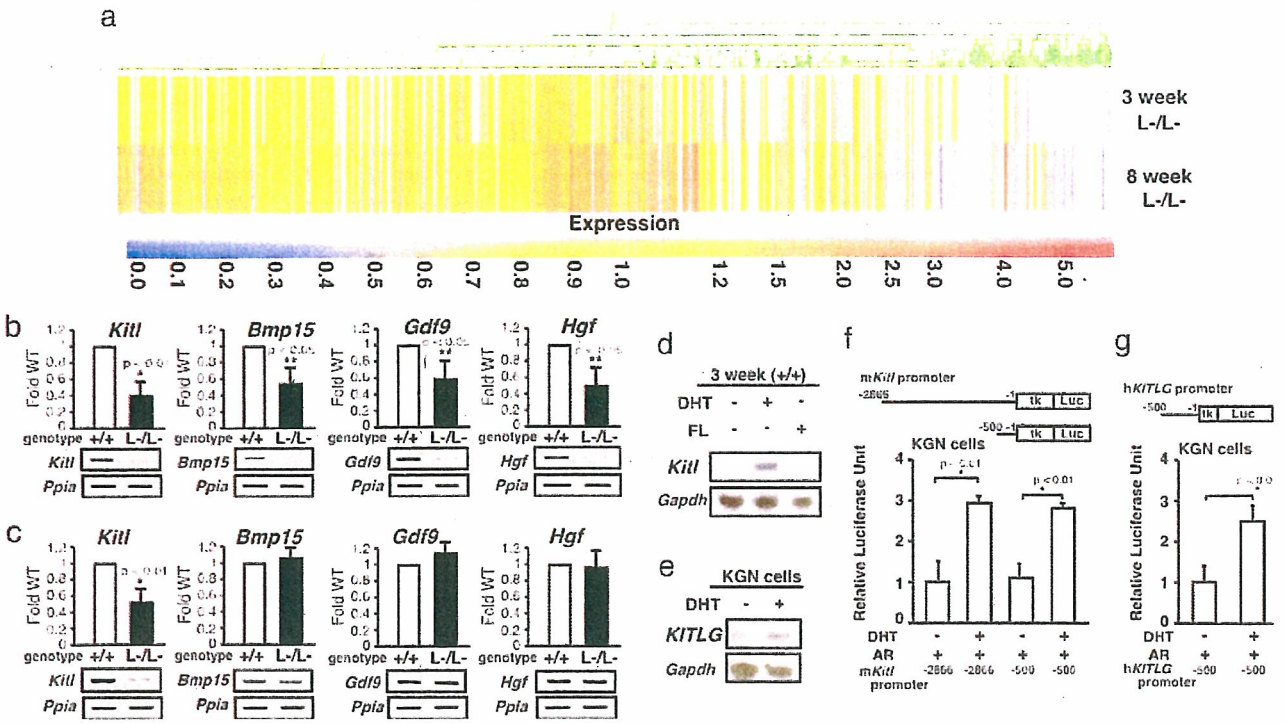

Fig. 4. Genome-wide microarray analysis and semiquantitative RT-PCR revealed that expression of the oocyte–granulosa cell regulator loop was down-regulated in $AR^{-/-}$ ovaries. (*a*) Microarray analysis of $AR^{-/-}$ compared with $AR^{+/+}$ ovaries at 3 and 8 weeks of age. Data obtained from microarray analysis as described in *Materials and Methods* were used to generate a cluster analysis. Each vertical line represents a single gene. The ratios of gene expression levels in $AR^{-/-}$ ovaries compared with wild type are presented. (*b* and *c*) Semiquantitative RT-PCR analysis of AR-regulated genes identified from the microarray study. Results shown are representative (using one ovary per genotype in each experiment) of five independent experiments. Data are shown as mean ± SEM and were analyzed by using Student's *t* test. (*d*) Comparison of *Kitl* gene expression by Northern blot analysis among placebo-, DHT-, and flutamide (FL)-treated $AR^{+/+}$ mouse ovaries. (*e*) Induction of *KITLG* gene expression by DHT treatment in KGN cells. (*f* and *g*) Androgen responsiveness in the mouse and human *kit ligand* promoters by a luciferase assay performed by using KGN cells. Data are shown as mean ± SEM and were analyzed by using Student's *t* test.

semiquantitative RT-PCR analysis (Fig. 3). Genome-wide microarray analysis (17) of RNA from 8-week-old $AR^{-/-}$ ovaries at the proestrus stage has been undertaken to identify AR-regulated genes. In comparison with $AR^{+/+}$ ovaries, expressions of 772 genes were down-regulated, whereas 351 genes were up-regulated in $AR^{-/-}$ ovaries (Fig. 4*a*; see also Tables 1 and 2, which are published as supporting information on the PNAS web site). Several genes known to be involved in the oocyte–granulosa cell regulatory loop (24) were identified as candidate AR target genes, including KIT ligand (*Kitl*) (25), morphogenetic protein 15 (*Bmp15*) (26), growth differentiation factor-9 (*Gdf9*) (27), and hepatocyte growth factor (*Hgf*) (28). Impaired folliculogenesis had been reported in mice deficient in each of these three regulators (26, 27, 29). To validate the microarray data, we performed semiquantitative RT-PCR analysis of 8-week-old $AR^{-/-}$ ovary RNA and confirmed that expression of these factors was down-regulated (Fig. 4*b*). To identify a regulator downstream of the AR signaling at an earlier stage of folliculogenesis, 3-week-old $AR^{-/-}$ ovaries that, as pointed out earlier, display no apparent phenotypic abnormality were examined. Fewer genes had altered expression levels (519 genes up-regulated; 326 genes down-regulated) (Fig. 4*a*; see also Tables 3 and 4, which are published as supporting information on the PNAS web site), and, of the four regulators tested by RT-PCR, only *Kitl* was found to be down-regulated at this age (Fig. 4*c*). Because *Kitl* is a granulosa cell-derived factor and stimulates oocyte growth and maturation (29–31), down-regulation of the *Kitl* expression in 3-week-old or even younger $AR^{-/-}$ ovaries may trigger impairment in folliculogenesis at a later age. To test for possible *Kitl* gene regulation by AR, 3-week-old wild-type females were treated with 5α-dihydrotestosterone (DHT). At 4 h after hormone injection, a clear induction of *Kitl* expression was observed in the ovaries, whereas a known antiandrogen flutamide attenuated the induction by DHT (Fig. 4*d*). The induction of endogenous human *kit ligand* (*KITLG*) gene by DHT was also observed in human granulosa-like tumor cells (KGN) in culture (Fig. 4*e*). Furthermore, androgen-induced transactivation of mouse and human *kit ligand* promoters (32) was observed by a luciferase reporter assay (33) in KGN (Fig. 4 *f* and *g*), 293T, and HeLa (data not shown) cells. However, no response to DHT was detected in the similar assay using promoters of the *Bmp15*, *Gdf9*, and *Hgf* genes (data not shown). Thus, we have shown that, in a regulatory cascade controlling folliculogenesis, *Kitl* represents a direct downstream target of androgen signaling.

As an upstream regulator, AR may also be indirectly involved in control of expression of other genes critical for folliculogenesis, because an age-dependent down-regulation of *Bmp15*, *Gdf9*, and *Hgf* gene expression was also observed in $AR^{-/-}$ ovaries. *Bmp15* and *Gdf9* are oocyte-derived factors that promote the development of surrounding granulosa cells in growing follicles (34, 35), whereas *Hgf* is secreted by theca cells and acts as a granulosa cell growth factor (36). Down-regulation of these factors, presumably due to decreased *Kitl* expression, may lead to impaired bidirectional communication between oocyte and granulosa cells (24) and, eventually, to early termination of folliculogenesis, as in POF syndrome.

Thus, we have identified AR as a novel regulator of follicu-

logenesis that apparently acts in the regulatory cascade upstream of the major factors controlling ovarian function, confirming the previous findings of the AR expression in granulose cells of growing follicles (3). Although not immediately relevant to the ovarian physiology, abnormal development of the mammary glands observed in our AR-deficient mice adds further strong evidence of an essential role of the AR not only in male, but also in female, reproductive function.

With increasing age of the first childbirth by women in the modern society, POF syndrome has become an important social and medical problem. Our findings suggest that POF syndrome may be caused by an impairment in androgen signaling and that X chromosomal mutations affecting the *AR* gene function may play a key role in hereditary POF. From clinical perspective, the present study provides evidence that AR can be a beneficial therapeutic target in treatment of POF syndrome patients.

We thank T. Iwamori and H. Tojo for expert advice on mammary gland anatomy, Y. Kanai for ovarian phenotypic analysis, members of the KO project team at the laboratory of Nuclear Signaling (Institute of Molecular and Cellular Biosciences) for their support, A. P. Kouzmenko for helpful suggestions, and H. Higuchi for manuscript preparation. This work was supported in part by the Program for Promotion of Basic Research Activities for Innovative Biosciences and priority areas from the Ministry of Education, Culture, Sports, Science, and Technology (to S.K.).

1. Laml, T., Preyer, O., Umek, W., Hengstschlager, M. & Hanzal, H. (2002) *Hum. Reprod. Update* **8,** 483–491.
2. Davison, R. M., Davis, C. J. & Conway, G. S. (1999) *Clin. Endocrinol. (Oxford)* **51,** 673–679.
3. Tetsuka, M., Whitelaw, P. F., Bremner, W. J., Millar, M. R., Smyth, C. D. & Hillier, S. G. (1995) *J. Endocrinol.* **145,** 535–543.
4. Ehrmann, D. A., Barnes, R. B. & Rosenfield, R. L. (1995) *Endocr. Rev.* **16,** 322–353.
5. Norman, R. J. (2002) *Mol. Cell. Endocrinol.* **191,** 113–119.
6. Kato, S. (2002) *Clin. Pediatr. Endocrinol.* **11,** 1–7.
7. Sato, T., Matsumoto, T., Kawano, H., Watanabe, T., Uematsu, Y., Sekine, K., Fukuda, T., Aihara, K., Krust, A., Yamada, T., *et al.* (2004) *Proc. Natl. Acad. Sci. USA* **101,** 1673–1678.
8. Sato, T., Matsumoto, T., Yamada, T., Watanabe, T., Kawano, H. & Kato, S. (2003) *Biochem. Biophys. Res. Commun.* **300,** 167–171.
9. Kawano, H., Sato, T., Yamada, T., Matsumoto, T., Sekine, K., Watanabe, T., Nakamura, T., Fukuda, T., Yoshimura, K., Yoshizawa, T., *et al.* (2003) *Proc. Natl. Acad. Sci. USA* **100,** 9416–9421.
10. Li, M., Indra, A. K., Warot, X., Brocard, J., Messaddeq, N., Kato, S., Metzger, D. & Chambon, P. (2000) *Nature* **407,** 633–636.
11. Sekine, K., Ohuchi, H., Fujiwara, M., Yamasaki, M., Yoshizawa, T., Sato, T., Yagishita, N., Matsui, D., Koga, Y., Itoh, N. & Kato, S. (1999) *Nat. Genet.* **21,** 138–141.
12. Yoshizawa, T., Handa, Y., Uematsu, Y., Takeda, S., Sekine, K., Yoshihara, Y., Kawakami, T., Arioka, K., Sato, H., Uchiyama, Y., *et al.* (1997) *Nat. Genet.* **16,** 391–396.
13. Gubbay, J., Collignon, J., Koopman, P., Capel, B., Economou, A., Munsterberg, A., Vivian, N., Goodfellow, P. & Lovell-Badge, R. (1990) *Nature* **346,** 245–250.
14. Yanagisawa, J., Yanagi, Y., Masuhiro, Y., Suzawa, M., Watanabe, M., Kashiwagi, K., Toriyabe, T., Kawabata, M., Miyazono, K. & Kato, S. (1999) *Science* **283,** 1317–1321.
15. Britt, K. L., Drummond, A. E., Cox, V. A., Dyson, M., Wreford, N. G., Jones, M. E., Simpson, E. R. & Findlay, J. K. (2000) *Endocrinology* **141,** 2614–2623.
16. Ohtake, F., Takeyama, K., Matsumoto, T., Kitagawa, H., Yamamoto, Y., Nohara, K., Tohyama, C., Krust, A., Mimura, J., Chambon, P., *et al.* (2003) *Nature* **423,** 545–550.
17. Fujimoto, N., Igarashi, K., Kanno, J., Honda, H. & Inoue, T. (2004) *J. Steroid Biochem. Mol. Biol.* **91,** 121–129.
18. Couse, J. F. & Korach, K. S. (1999) *Endocr. Rev.* **20,** 358–417.
19. Elvin, J. A. & Matzuk, M. M. (1998) *Rev. Reprod.* **3,** 183–195.
20. Hu, Y. C., Wang, P. H., Yeh, S., Wang, R. S., Xie, C., Xu, Q., Zhou, X., Chao, H. T., Tsai, M. Y. & Chang, C. (2004) *Proc. Natl. Acad. Sci. USA* **101,** 11209–11214.
21. Elvin, J. A., Yan, C., Wang, P., Nishimori, K. & Matzuk, M. M. (1999) *Mol. Endocrinol.* **13,** 1018–1034.
22. Zhou, J., Kumar, T. R., Matzuk, M. M. & Bondy, C. (1997) *Mol. Endocrinol.* **11,** 1924–1933.
23. Burns, K. H., Yan, C., Kumar, T. R. & Matzuk, M. M. (2001) *Endocrinology* **142,** 2742–2751.
24. Matzuk, M. M., Burns, K. H., Viveiros, M. M. & Eppig, J. J. (2002) *Science* **296,** 2178–2180.
25. Joyce, I. M., Pendola, F. L., Wigglesworth, K. & Eppig, J. J. (1999) *Dev. Biol.* **214,** 342–353.
26. Yan, C., Wang, P., DeMayo, J., DeMayo, F. J., Elvin, J. A., Carino, C., Prasad, S. V., Skinner, S. S., Dunbar, B. S., Dube, J. L., *et al.* (2001) *Mol. Endocrinol.* **15,** 854–866.
27. Dong, J., Albertini, D. F., Nishimori, K., Kumar, T. R., Lu, N. & Matzuk, M. M. (1996) *Nature* **383,** 531–535.
28. Parrott, J. A., Vigne, J. L., Chu, B. Z. & Skinner, M. K. (1994) *Endocrinology* **135,** 569–575.
29. Driancourt, M. A., Reynaud, K., Cortvrindt, R. & Smitz, J. (2000) *Rev. Reprod.* **5,** 143–152.
30. Huang, E. J., Manova, K., Packer, A. I., Sanchez, S., Bachvarova, R. F. & Besmer, P. (1993) *Dev. Biol.* **157,** 100–109.
31. Packer, A. I., Hsu, Y. C., Besmer, P. & Bachvarova, R. F. (1994) *Dev. Biol.* **161,** 194–205.
32. Grimaldi, P., Capolunghi, F., Geremia, R. & Rossi, P. (2003) *Biol. Reprod.* **69,** 1979–1988.
33. Kitagawa, H., Fujiki, R., Yoshimura, K., Mezaki, Y., Uematsu, Y., Matsui, D., Ogawa, S., Unno, K., Okubo, M., Tokita, A., *et al.* (2003) *Cell* **113,** 905–917.
34. Otsuka, F. & Shimasaki, S. (2002) *Proc. Natl. Acad. Sci. USA* **99,** 8060–8065.
35. Joyce, I. M., Clark, A. T., Pendola, F. L. & Eppig, J. J. (2000) *Biol. Reprod.* **63,** 1669–1675.
36. Parrott, J. A. & Skinner, M. K. (1998) *Endocrinology* **139,** 2240–2245.

Available online at www.sciencedirect.com
ScienceDirect
Biochemical and Biophysical Research Communications 352 (2007) 164–169
BBRC
www.elsevier.com/locate/ybbrc

A novel embryotoxic estimation method of VPA using ES cells differentiation system

Mayu Murabe, Junji Yamauchi, Yoko Fujiwara, Masami Hiroyama, Atsushi Sanbe, Akito Tanoue *

Department of Pharmacology, National Research Institute for Child Health and Development, Setagaya, Tokyo 157-8535, Japan

Received 26 October 2006
Available online 13 November 2006

Abstract

Valproic acid (VPA), which has a wide range of therapeutic applications, is known as a potent teratogen that induces neural tube defects in vertebrates. Here, we have characterized the tissue-specific, embryotoxic effects of VPA on developmental processes using a novel system with differentiating mouse ES cells. Under our cultivating condition, ES cells differentiated into cardiomyocytes, although various cell types can be differentiated. VPA affected cell viability and differentiation from undifferentiated ES cells to cardiomyocytes in a dose-dependent manner. The analysis of tissue-specific markers also revealed that VPA potently inhibited mesodermal and endodermal development but promoted neuronal differentiation in a lineage-specific manner. Taking the *in vivo* teratogenicity of VPA into account, this assay system could be useful in predicting the degree of embryotoxicity of VPA. We, thus, propose that the *in vivo* embryotoxic effects of various medicines can be estimated fast and accurately using this *in vitro* cell differentiation system.

Keywords: ES cell; Valproic acid; Embryotoxicity

Valproic acid (VPA) is a short-chained fatty acid with a broad spectrum of antiepileptic activities and it is also used in migraine prophylaxis and the treatment of bipolar disorders, neuropathic pain [1,2]. It is also being tried as an anticancer agent. VPA, which has a wide range of therapeutic applications, is also a potent teratogen and is associated with elevated risks for neural, craniofacial, cardiovascular, and skeletal birth defects [3,4]. The predominant VPA-induced teratogenic effects are due to failure of the neural tube to close (neural tube defects, NTDs), leading to conditions such as spina-bifida-aperta, anencephaly, and exencephaly in humans, mice, and other vertebrates [3,5–7].

In this study, we attempted to characterize the tissue-specific embryotoxicity of VPA using a system with mouse embryonic stem (ES) cell differentiation. This *in vitro* embryotoxicity assay requires a simple procedure that can be accomplished in a shorter time (10 days) [8] than that required by other assays used in developmental toxicological studies with experimental animals. Since ES cells are undifferentiated pluripotent embryo-derived stem cell lines and are capable to develop into differentiated cell types representing endodermal, ectodermal, and mesodermal lineages, ES cells lines are very suitable to analyze the mutagenic, cytotoxic, and embryotoxic effects of chemical compounds *in vitro* [9]. By analyzing the expression of tissue-specific genes and conducting histological and immunocytochemical studies, we have demonstrated that VPA inhibits the differentiation of mesodermal and endodermal lineages. On the other hand, VPA can induce neural differentiation in a lineage-specific manner. It is conceivable that these abnormalities of tissue developments in ES cells reflect the embryotoxic effects of VPA *in vivo*. Using this *in vitro* embryotoxicity estimation system, it would be possible to predict the effects of chemicals on developmental processes *in vivo* in a short time.

* Corresponding author. Fax: +81 3 5494 7057.
E-mail address: atanoue@nch.go.jp (A. Tanoue).

0006-291X/$ - see front matter © 2006 Elsevier Inc. All rights reserved.
doi:10.1016/j.bbrc.2006.10.189

Materials and methods

Materials. The following antibodies were purchased: anti-troponin I from Chemicon (Temecula, CA), anti-albumin from Bethyl Laboratory (Montgomery, TX), and anti-neurofilament 200 from Sigma–Aldrich (St. Louis, MO).

ES cell culture. Mouse ES cells (R1) were maintained and used for differentiation as previously described [10]. ES cells were grown on 0.1% gelatin-coated tissue culture dishes in a standard ES-cell culture medium-containing D-MEM supplemented with 10% FCS, 2 mM glutamine, 0.1 mM non-essential amino acids, 0.1 mM β-mercaptoethanol, 1000 U/ml LIF (Chemicon, Temecula, CA), 50 U/ml penicillin G, and 50 μg/ml streptomycin. For the differentiation of R1 ES cells, we followed the method of the embryonic stem cell test (EST) [8]. In brief, ES cells were suspended in an ES-differentiation medium-containing D-MEM supplemented with 20% FCS, 2 mM glutamine, 0.1 mM non-essential amino acids, 0.1 mM β-mercaptoethanol, 50 U/ml penicillin G, and 50 μg/ml streptomycin and cultivated in hanging drops ($n = 500$) as aggregates (called embryoid bodies (EBs)) for 3 days [10]. The EBs were transferred to suspension culture dishes (Sumitomo Bakelite, Tokyo, Japan) and cultured for 2 days. They ($n = 1$/well) were plated onto a 24-well tissue culture plate on day 5 and incubated for 5 additional days. To estimate the differentiating efficiencies from ES cells into cardiomyocytes, the distinctive beating movements of differentiated cardiomyocytes were analyzed under an inverted phase-contrast microscope (Nikon, Tokyo, Japan).

Cytotoxicity assay. For the cytotoxicity assay, we followed the method of the embryonic stem cell test (EST) [8]. ES cells and NIH-3T3 fibroblasts (1×10^4 cells/ml) were seeded in a volume of 50 μl/well into a 96-well flat-bottomed tissue culture microtiter plate and incubated in a humidified atmosphere with 5% CO_2 at 37 °C for 2 h. After incubation, 150 μl of a culture medium-containing the appropriate dilution of test chemicals was added. On day 3 and day 5, the culture medium was removed, and, subsequently, 200 μl of the same concentration of the test substance used on day 1 was added to the microtiter plates. On day 10, the methylthiazolyldiphenyl-tetrazolium bromide (MTT) cytotoxicity assay [11] was carried out [8]. A volume of 20 μl of 5 mg/ml 3-[4,5-dimethylthiazol-2-yl]-2,5-diphenyl-tetrazolium bromide, MTT (Sigma–Aldrich, St. Louis, MO), in PBS was added into each microtiter well and incubated in a humidified atmosphere with 5% CO_2 at 37 °C for 2 h. After removal of the supernatant, cells were incubated with 130 μl of a desorb-mix solution-containing 3.49% (v/v) of a 20% SDS aqueous solution and 96.51% (v/v) 2-propanol. After agitation for 15 min on an N-704 microtiter plate shaker (Nissin, Tokyo, Japan), the plates were transferred to a Wallac 1420 multi-label counter (Perkin-Elmer, Wellesley, MA), and the absorbance of each well at a wavelength of 520 nm and a reference wavelength of 630 nm was examined. Representative results from three separate experiments are shown in the figure. For morphological observations, samples on day 5 were examined using a Hoffman differential interference contrast microscope.

Immunocytochemistry. On day 3 of the differentiation assay, several EBs were cultured on 0.1% gelatin-coated glass-based 60 mm dishes. After changing the media on day 5, the cells of day 10 were fixed with 4% paraformaldehyde for 20 min at room temperature. After rinsing with PBS twice, samples were pretreated with PBS-containing 0.2% Triton X-100 in PBS for 30 s. After washing with PBS twice, the samples were incubated with PBS-containing 0.1 M glycine, pH 3.5, for 30 min, rinsed with PBS twice, and blocked in PBS-containing 1% BSA, 0.1% gelatin, and 0.1% Tween 20 for 1 h at room temperature. They were incubated at 4 °C overnight with the following antibodies: anti-troponin I (mouse IgG, 1:500), anti-albumin (goat IgG, 1:500), and anti-neurofilament 200 (rabbit IgG, 1:500). After washing with PBS three times, the cells were incubated for 1 h at room temperature with secondary antibodies conjugated with Alexa 488 (Invitrogen, Carlsbad, CA). After washing with PBS three times, the samples were mounted with the Vectashield mounting medium with DAPI (Vector Laboratories, Burlingame, CA) and examined with an FV500 confocal laser scanning microscope (Olympus, Tokyo, Japan). To estimate the differentiating efficiencies from ES cells into neuronal cells, NF-positive cells (neurons) were counted against DAPI-positive cells (~200 cells) under an inverted phase-contrast microscope (Nikon, Tokyo, Japan). Representative results from three separate experiments are shown in the figure.

RNA isolation, cDNA synthesis, and RT-PCR. Total RNA was extracted from samples on day 10 of the differentiation assay using the RNA extraction kit ISOGEN (Nippon Gene, Tokyo, Japan) and digested with deoxyribonuclease (RT Grade) (Nippon Gene, Tokyo, Japan) to remove any contaminating genomic DNA. The concentration of RNA was measured with a BioSpec-mini DNA/RNA/protein analyzer (Shimazu, Kyoto, Japan). cDNA was synthesized with the use of 3 μg of RNA, 500 ng of oligo-dT12-18 primers, and 200 U of SuperScript III reverse transcriptase (Invitrogen, Carlsbad, CA). To analyze the relative expression of different mRNAs, the amount of cDNA was normalized on the basis of the signals from ubiquitously expressed β-actin mRNA. PCR was carried out using an Ex-Taq kit (Takara Bio, Shiga, Japan) according to the manufacturer's standard protocol in a final volume of 25 μl. The primer sequences are summarized in Table 1.

Table 1
PCR primers for the detection of tissue-specific marker gene expressions used in this study

Gene	Sequences (5′–3′)		Product length (bp)
	Forward	Reverse	
Oct4	GGTGGAGGAAGCCGACAAC	TTCGGGCACTTCAGAAACATG	141
Sox2	AGATGCACAACTCGGAGATCAG	CCGCGGCCGGTATTTATAAT	146
BMP4	CTGCCGTCGCCATTCACTAT	TGGCATGGTTGGTTGAGTTG	146
Nkx2.5	CCAAGTGCTCTCCTGCTTTCC	CCATCCGTCTCGGCTTTGT	148
MLC-2v	GCTTCATCGACAAGAATGAC	GAATGCGTTGAGAATGGTCT	185
ANF	CGGTGTCCAACACAGATCTG	TCTCTCAGAGGTGGGTTGAC	187
MyoD	ACGGCTCTCTCTGCTCCTTTG	CGTGCTCCTCCGGTTTCA	138
GATA6	CGGTCATTACCTGTGCAATG	GCATTTCTACGCCATAAGGTA	159
TTR	GTCCTCTGATGGTCAAAGTC	TCCAGTTCTACTCTGTACAC	193
HNF1	AGCCGCAGAACCTTATCATG	GGTTGGTGTCTGTGATCAAC	390
AFP	ACTCACCCCAACCTTCCTGTC	CAGCAGTGGCTGATACCAGAG	422
ALB	GGAACTTGCCAAGTACATGTGTGA	CAGCAATGGCAGGCAGATC	146
Nestin	TGCATTTCCTTGGGATACCAG	CTTCAGAAAGGCTGTCACAGGAG	122
Synaptophysin	GTGGAGTGTGCCAACAAGAC	ATTCAGCCGAGGAGGAGTAG	158
NFH	AGGACCGTCATCAGGCAGACATTGC	GACCAAAGCCAATCCGACACTCTTC	201
GFAP	TGCCACGCTTCTCCTTGTCT	GCTAGCAAAGCGGTCATTGAG	146
Olig2	TGCGCCTGAAGATCAACAG	CATCTCCTCCAGCGAGTTG	182
DM20	TGAAGCTCTTCACTGGTACAG	GTCTTGTAGTCGCCAAAGAT	207
β-Actin	GCTCTGGCTCCTAGCACCAT	GGGCCGGACTCATCGTACT	146

Quantitative RT-PCR. For quantitative RT-PCR, gene expression was assessed by real-time PCR with the use of a 7900HT Fast Real-Time PCR System (Applied Biosystems, Foster City, CA). The reaction mixtures contained 1 μl of template cDNA with 100 nM of forward and reverse primers and 10 μl of SYBR Premix Ex Taq (Takara Bio, Shiga, Japan) in a total volume of 20 μl. Duplicate assays were run for each sample, and each included a standard curve and a negative control. Specific oligonucleotide primers were designed to produce 122- to 422-bp products. The amplification protocol consisted of 10 min at 95 °C followed by 40 cycles at 95 °C for 15 s and 60 °C for 1 min. The relative quantitative expressions of tissue-specific markers, after normalization with GAPDH as a housekeeping gene, were calculated. The primer sequences are summarized in Table 1. The primers for GAPDH were purchased from Applied Biosystems (Foster City, CA).

Results

The cell viability assay (MTT assay) was used to study the cytotoxic effect of VPA with ES cells, representing embryonic tissues, and NIH-3T3 fibroblasts, representing adult tissues. In both cell lines, VPA inhibited the survival of cells in a dose-dependent manner (Fig. 1). However, there was a significant difference in cytotoxic sensitivities against VPA between ES cells and NIH-3T3 fibroblasts. The IC_{50} values, the inhibitory concentration of 50% cell viability, were calculated at 3.25 and 0.56 mM for NIH-3T3 fibroblasts and ES cells, respectively. The therapeutic range of VPA is 0.30–0.70 mM in serum. The IC_{50} value of NIH-3T3 fibroblasts, 3.25 mM, was approximately 5–11 times the therapeutic concentration. In contrast, the IC_{50} of ES cells, 0.56 mM, was within the therapeutic range of VPA. Since ES cells are more significantly affected by the therapeutic range of VPA than NIH-3T3 fibroblasts, developing cells during embryogenesis could be seriously damaged by the VPA therapeutic concentration. To observe the cytotoxic and morphological effects of VPA on ES cells and NIH-3T3 fibroblasts, ES cells and NIH-3T3 fibroblasts colored with the MTT were observed on day 5 of the cytotoxicity assay (Fig. 1). In both cell lines, the cell densities were gradually reduced in a concentration-dependent manner. In a high-medication group, NIH-3T3 fibroblasts showed strong indications of shrinking. However, in ES cells, many small cells, considered as undifferentiated cells, showed strong signs of inhibition to differentiation.

To characterize the tissue-specific effects of VPA on the ES differentiation system at the molecular levels, the expression levels of typical tissue-specific genes were examined using RT-PCR analysis with samples on day 10 of the differentiation assay (Supplemental Fig.1). In this culture condition-containing 20% FCS, ES cells were mainly differentiated into endodermal and mesodermal lineages, such as cardiomyocytes, but not into ectodermal lineages, such as neural cells. This is in agreement with the fact that some growth factors involved in FCS are known to inhibit the neural induction of various kinds of adult neural stem cells. Oct4, a representative undifferentiated marker, was highly detected in all samples of high VPA concentrations. Other primitive markers, such as BMP4 (a mesodermal marker), GATA6 (an endodermal marker), and Nestin (an ectodermal, neural marker), were also strongly detected in the samples with high VPA concentrations. In contrast, VPA reduced the expression levels of late-stage markers, such as Nkx2.5 and MLC-2v (cardiomyocyte markers) and TTR, HNF1, AFP, and albumin (ALB) (endodermal markers), whereas Synaptophysin (Syn), a typical neural marker, was increased in a VPA concentration-dependent manner. No expression of MyoD (a muscle marker) and GFAP (a glial marker) was detected. These results suggest a tendency for VPA to inhibit the differentiation into

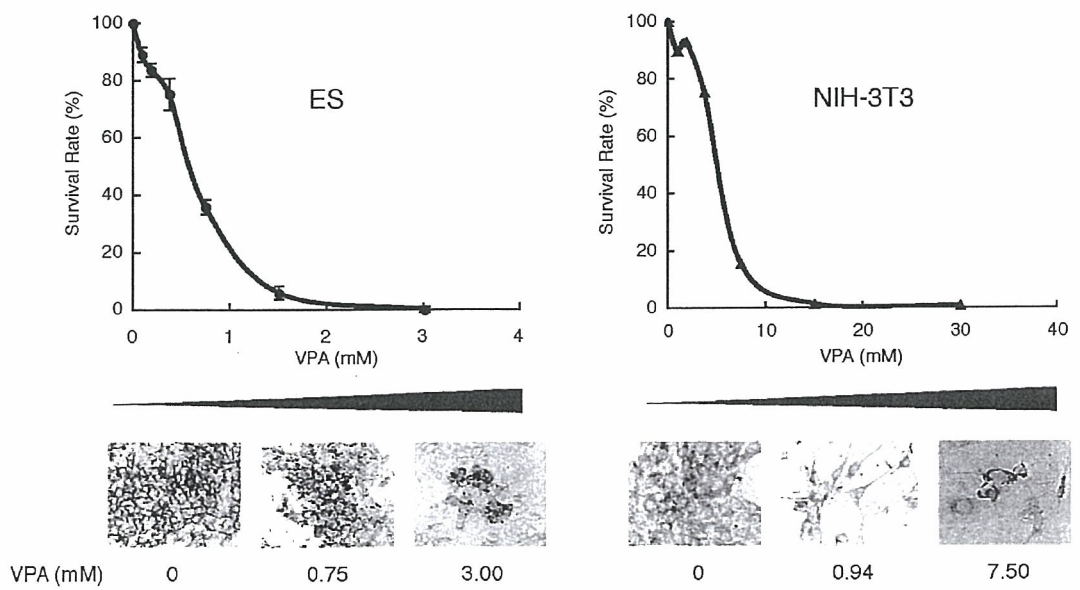

Fig. 1. Cytotoxicity assay for ES cells and NIH-3T3 fibroblasts. Cells on day 10 of the assay were stained with the MTT and solubilized. The activity of the mitochondrial enzyme of living cells was examined. The violet color of the MTT formazan, which is the enzyme product, was measured with the absorbance of 520 nm. On day 5, cells were stained with the MTT and examined with a Hoffman differential interference contrast microscope.

cardiomyocytes and endodermal lineages and to adversely induce differentiation into neural lineages. Undifferentiated ES cells also remained under a condition of high VPA concentration.

To characterize the VPA effects more closely, we performed quantitative expression analysis of tissue-specific genes and immunocytochemical or morphological analysis with samples on day 10 of the differentiation assay (Figs. 2 and 3). It was demonstrated that the expression levels of Oct4 and Sox2 (undifferentiated markers) were high under the condition of high VPA concentration (Fig. 2A-(1)). For mesodermal lineages, the expressions of BMP4, Nkx2.5, MLC-2v, and ANF were reduced, and MyoD was not detected (Fig. 2A-(2)). On day 10 of the differentiation assay, cardiomyocytes were normally differentiated (Fig. 2C, left). The number of cells stained with an antibody against troponin I (a typical cardiomyocyte-specific marker) was decreased notably under the conditions of high VPA concentration (data not shown). The ratio of induced cardiomyocytes was determined from their autonomous

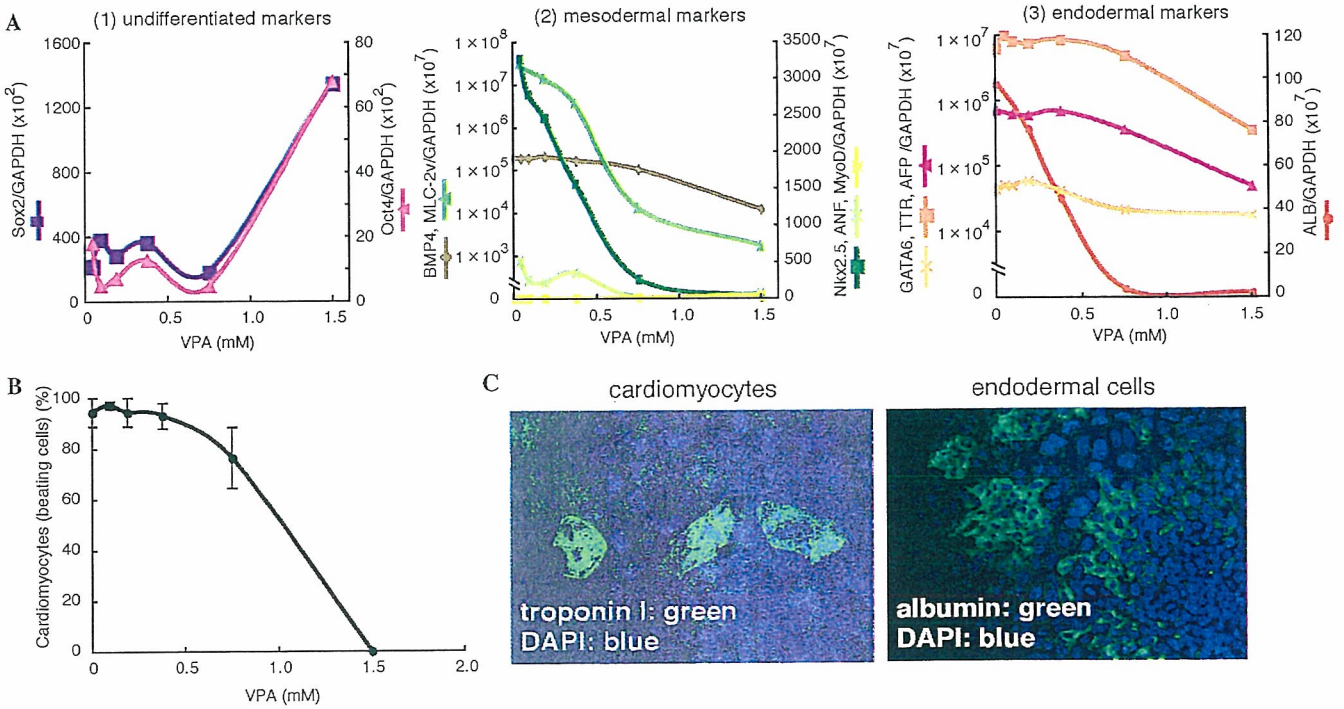

Fig. 2. ES differentiation assay 1: the undifferentiated state and mesodermal and endodermal differentiation. (A) The expression levels of typical undifferentiated markers, Oct4 and Sox2 (1), mesodermal markers, BMP4, MLC-2v, Nkx2.5, ANF, and MyoD (2), and endodermal markers, GATA6, TTR, AFP, and ALB (3), were quantified at each concentration of VPA with real-time RT-PCR. (B) Cardiomyocytes derived from ES cells were analyzed by observing their distinctive beating movements at each concentration of VPA. (C) (left) Cardiomyocytes were immunostained with an anti-troponin I antibody. (right) Endodermal cells derived from ES cells were immunostained with an anti-albumin antibody.

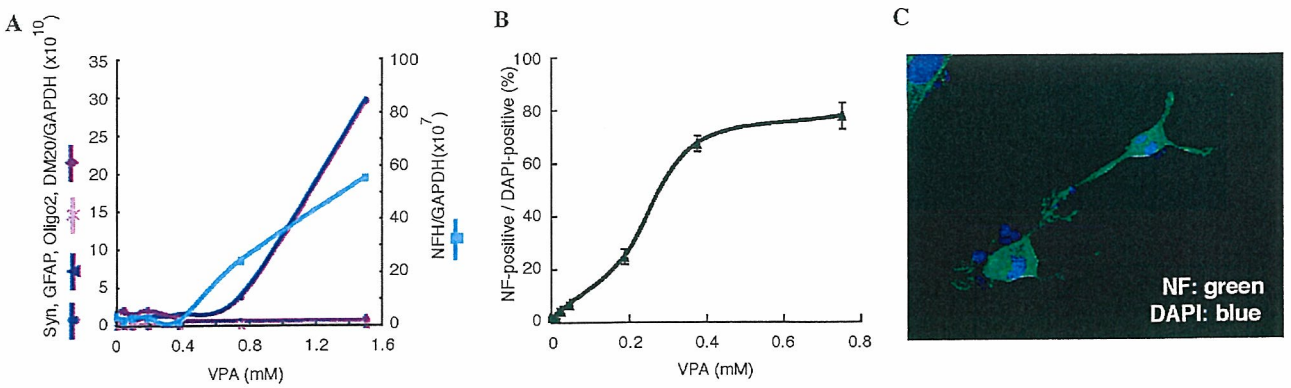

Fig. 3. ES differentiation assay 2: ectodermal differentiation. (A) The expression levels of typical ectodermal markers, Synaptophysin, NFH, GFAP, and Oligo2, were quantified with real-time RT-PCR. (B) The efficiency of neuronal differentiation from ES cells was estimated with anti-neurofilament antibody-stained cells (NF-positive) against total cells (DAPI-positive). (C) Neuronal cells derived from ES cells (VPA 0.38 mM) were immunostained with an anti-neurofilament (NF) 200 antibody.

contractile motions and was shown to decrease in a concentration-dependent manner (Fig. 2B). It was also confirmed that VPA inhibited the differentiation into cardiomyocytes at the molecular and morphological levels. On day 10 of the differentiation assay, a cellular population expressed a definitive endodermal marker, ALB was detected (Fig. 2C, right). The expression levels of GATA6, TTR, AFP, and ALB were decreased in a concentration-dependent manner (Fig. 2A-(3)), suggesting that VPA suppressed the differentiation into endodermal lineages. For ectodermal lineages, the expression levels of neuron-specific markers, such as Synaptophysin (Syn) and NFH, were increased in a concentration-dependent manner. Glial markers, such as GFAP, which is a representative astrocyte-specific marker, and Oligo2 and DM20, which are oligodendrocyte-specific markers, were not induced (Fig. 3A). With a dose of 0.38 mM VPA, many positive cells to neurofilament 200, which is a neuron-specific marker, were detected in samples on day 10 of the differentiation assay (Fig. 3C), and the ratio of anti-neurofilament 200-positive cells was increased in a concentration-dependent manner (Fig. 3B). On the other hand, cells stained with the anti-GFAP antibody were not observed (data not shown). Taken together, these results suggest that VPA promotes ES cells to differentiate into neurons but not glial cells.

Discussion

In the cell viability assay, there was a significant difference in the sensitivities against VPA between ES cells as an embryonic tissue cell model and NIH-3T3 fibroblasts as an adult tissue cell model. VPA has been in clinical use as a safe and effective antiepileptic drug (AED) in a wide range of epileptic conditions in children and adults [12]. Although VPA has been shown to have very few side effects, it is a potent teratogen and produces several malformations in embryos [5,13,14]. Thus, VPA could affect embryonic tissue cells more than adult tissue cells and, consequently, might cause damage to developing cells and, specifically, to embryos. In fact, VPA caused triploblastic differentiations of ES cells in the study herein reported.

Here, we showed that VPA stimulated the differentiation of ES cells into neuronal cells in a lineage-specific manner but attenuated the differentiation of ES cells into endodermal or mesodermal cells. Similarly to this finding in ES cells, VPA is known to promote neuronal fate and to inhibit glial fate simultaneously in multiple adult neural progenitor cells [15]. Whereas VPA can promote the differentiation of the adult neural progenitor cell by induction of neurogenic transcription factors such as NeuroD [15], it remains to be determined what mechanisms of the neuronal differential promotion are involved in ES cells. Nevertheless, it seemed that the altered development of neural cells or tissues driven by VPA could result in NTDs [4], which are predominant VPA-induced teratogenic malformations.

VPA has been reported to inhibit histone deacetylases (HDACs) in a therapeutic range (0.30–0.70 mM) and cause the hyperacetylation of histones in HeLa, F9 teratocarcinoma, and Neuro2A neuroblastoma cells [16,17]. In general, increased levels of histone acetylation are associated with increased transcriptional activity, whereas decreased levels of acetylation are associated with the repression of gene expression [18,19]. A number of specific and potent inhibitors of HDACs, such as trichostatin A (TSA) and VPA, prevent tumorigenesis in rodent and human models and have potential therapeutic roles in the treatment of malignant diseases [20,21]. Furthermore, VPA has been reported to arrest the cell cycle at a G0/1 phase, inhibit proliferation, and induce apoptosis in multiple myeloma [22,23] *in vitro*. Thus, VPA could also inhibit cell proliferation in ES cells by a similar mechanism. In addition, it is also accepted that HDACs play an important role during the embryogenesis of numerous organisms, and interfering with their functions using HDAC inhibitors, such as VPA, could result in some developmental abnormalities, such as teratogenicity [24]. These findings suggest that the effects of VPA on cell growth and neurons might be via the inhibition of HDACs.

Recently, stem cells have become important new tools for the development of *in vitro* model systems to test drugs and chemicals and have shown potential to predict or estimate toxicity [25]. Among various stem cells, ES cells are some of the most valuable cells to develop *in vitro* model systems because they are capable of self-renewing and differentiating into every cell type of the mammalian organism and therefore have higher plasticity than adult stem cells. Since mouse ES cells are prone to differentiate into cardiomyocytes, drug toxicity, such as cardiotoxicity, can be assessed using ES cells [26–30]. The embryonic stem cell test (EST) is an *in vitro* embryotoxicity assay that assesses the ability of chemical compounds to inhibit the differentiation of ES cells into cardiomyocytes [31,32]. In comparison to *in vivo* studies, EST is easy and highly accurate in predicting cellular toxicity, outperforming classical assays, such as fetal limb micromass and post-implantation whole-rat embryo cultures [32]. Thus, EST is a simple and accurate test for toxicity; however, it is not sufficient for evaluating all chemicals because only two parameters of cytotoxicity and morphological change are assessed in the reported EST [8]. Therefore, we attempted to characterize the tissue-specific embryotoxicity of VPA by analyzing the gene expression of the tissue-specific markers as well as by conducting a histological and immunocytochemical study and examining the established two parameters in the mouse embryonic stem (ES) cell differentiation system. Using this system, we demonstrated that VPA is highly cytotoxic and potent to inhibit differentiation into cardiomyocytes in a cytotoxicity and morphological study as well as stimulates the differentiation of the neuronal lineage and inhibits the differentiation of mesodermal and endodermal lineages. Taking the *in vivo* embryotoxicity of VPA into account, the system presented in this study could be useful for predicting the degree of the abnormal neural development of VPA *in vivo*.

In conclusion, this *in vitro* ES cell system allows estimating and characterizing the embryotoxic effects of various chemicals. Further research on this innovative method may help to establish high-throughput screening analysis of drugs to reduce the number of experimental animals and save time.

Acknowledgments

This work was supported in part by research grants from the Scientific Fund of the Ministry of Education, Science, and Culture of Japan, the Ministry of Human Health and Welfare of Japan, and the Japan Health Science.

Appendix A. Supplementary data

Supplementary data associated with this article can be found, in the online version, at doi:10.1016/j.bbrc.2006.10.189.

References

[1] B.F.D. Bourgeois, Valproic Acid—Clinical Efficacy and Use in Epilepsy, in: R.H. Levy, R.H. Mattson, B.S. Meldrum, E. Perucca (Eds.), Antiepileptic Drugs, Lippincot Williams & Wilkins, Philadelphia, 2002, pp. 808–817.

[2] S.D. Silberstein, Clinical Efficacy and Use in Other Neurological Disorders, in: R.H. Levy, R.H. Mattson, B.S. Meldrum, E. Perucca (Eds.), Antiepileptic Drugs, Lippincot Williams & Wilkins, Philadelphia, 2002, pp. 818–827.

[3] H. Nau, R.S. Hauck, K. Ehlers, Valproic acid-induced neural tube defects in mouse and human: aspects of chirality, alternative drug development, pharmacokinetics and possible mechanisms, Pharmacol. Toxicol. 69 (1991) 310–321.

[4] H. Nau, Valproic acid-induced neural tube defects, CIBA Found. Symp. 181 (1994) 144–160.

[5] E.J. Lammer, L.E. Severr, G.P. Oakley Jr., Teratogen update: valproic acid, Teratology 35 (3) (1987) 465–473.

[6] A. Oberemm, F. Kirchbaum, Valproic acid induced abnormal development of the central nervous system of three species of amphibians: implications for neural tube defects and alternative experimental systems, Teratogen. Carcin. Mutagen. 12 (6) (1992) 251–262.

[7] A.I. Whitsel, C.B. Johnson, C.J. Forehand, An *in ovo* chicken model to study the systemic and localized teratogenic effects of valproic acid, Teratology 66 (4) (2002) 153–163.

[8] H. Spielmann, I. Pohl, B. Dröing, M. Liebsch, F. Moldenhauer, The embryonic stem cell test, *in vitro* embryotoxicity test using two permanent mouse cell lines: 3T3 fibroblast and embryonic stem cells, In Vitro Toxicol. 10 (1997) 119–127.

[9] J. Rohwedel, K. Guan, C. Hegert, A.M. Wobus, Embryonic stem cells as an *in vitro* model for mutagenicity, cytotoxicity and embryotoxicity studies: present state and future, Toxicol. In Vitro 15 (2001) 741–753.

[10] A.M. Wobus, K. Guan, H.T. Yang, K. Boheler, Embryonic Stem Cells: Methods and Protocols, in: K. Turksen (Ed.), Methods in Molecular Biology, Humana, Totowa, NJ, 2002, pp. 127–156.

[11] T. Mosman, Rapid colorimetric assay for cellular growth and survival: application to proliferation and cytotoxicity assays, J. Immunol. Methods 65 (1983) 55–63.

[12] E. Lepkifker, I.D.P. Iancu, R. Ziv, M. Kotler, Valproic acid in ultra-rapid cycling, Clin. Neuropharmacol. 18 (1995) 72–75.

[13] H. Nau, R. Zierer, H. Spielmann, D. Neubert, C. Gansau, A.H. van Gennip, A new model for embryotoxicity testing: teratogenicity and pharmacokinetics of valproic acid following constant-rate administration in the mouse using human therapeutic drug and metabolite concentrations, Life Sci. 29 (1981) 2803–2814.

[14] K. Wide, B. Winbladh, B. Kallen, Major malformations in infants exposed to antiepileptic drugs in utero, with emphasis on carbamazepine and valproic acid: a nation-wide, population-based register study, Acta Paediatr. 93 (2004) 174–176.

[15] J. Hsieh, K. Nakashima, T. Kuwabara, E. Mejia, F.H. Gage, Histone deacetylase inhibition-mediated neuronal differentiation of multipotent adult neural progenitor cells, Proc. Natl. Acad. Sci. USA 101 (2004) 16659–16664.

[16] R.A. Blaheta, J. Cinatl Jr., Anti-tumor mechanisms of valproate: a novel role for an old drug, Med. Res. Rev. 22 (2002) 492–511.

[17] M. Kaiser, I. Zavrski, J. Sterz, C. Jakob, C. Fleissner, P-M. Kloetzel, O. Sezer, U. Heider, The effects of the Histone deacetylase inhibitor valproic acid on cell cycle, growth suppression and apoptosis in multiple myeloma, Haematologica 91 (2006) 248–251.

[18] M. Gottlicher, S. Minucci, P. Zhu, O.H. Kramer, H.A. Schimpf, S. Giavara, J.P. Sleeman, F. Lo Coco, C. Nervi, P.G. Pelicci, T. Heinzel, Valproic acid defines a novel class of HDAC inhibitors inducing differentiation of transformed cells, EMBO J. 20 (2001) 6969–6978.

[19] C.J. Phiel, F. Zhang, E.Y. Huang, M.G. Guenther, M.A. Lazar, P.S. Klein, Histone deacetylase is a direct target of valproic acid, a potent anticonvulsant, mood stabilizer, and Teratogen, J. Biol. Chem. 276 (2001) 36734–36741.

[20] A.J.M. De Ruijter, A.H. van Gennip, H.N. Caron, S. Kemp, A.B.P. van Kuilenburg, Histone deacetylases (HDACs): characterization of the classical HDAC family, Biochem. J. 370 (2003) 737–749.

[21] R.W. Johnstone, Histone deacetylase inhibitors: novel drugs for the treatment of cancer, Nat. Rev. Drug Discov. 1 (2002) 287–299.

[22] R.J. Lin, T. Sternsdorf, M. Tini, R.M. Evans, Transcriptional regulation in acute promyelocitic leukemia, Oncogene 20 (2001) 7204–7215.

[23] P.P. Pandolfi, Transcriptional therapy for cancer, Oncogene 20 (2001) 3116–3127.

[24] E. Menegola, F. Di Renzo, M.L. Broccia, M. Prudenziati, S. Minucci, V. Massa, E. Giavini, Inhibition of histone deacetylase activity on specific embryonic tissues as anew mechanism for teratogenicity, Birth Defects Res. (part B) 74 (2005) 392–398.

[25] J.C. Davila, G.G. Cezar, M. Thiede, S. Strom, T. Miki, J. Trosko, Use and application of stem cells in toxicology, Toxicol. Sci. 79 (2004) 214–223.

[26] I. Kehat, D. Kenyagin-Karsenti, M. Snir, H. Segev, M. Amit, A.S. Gepstein, E. Livne, O. Binah, J. Itskovitz-Eldor, L. Gepstein, Human embryonic stem cells can differentiate into myocytes with structural and functional properties of cardiomyocytes, J. Clin. Invest. 108 (2001) 407–414.

[27] I. Kehat, A. Gepstein, A. Spira, J. Itskovitz-Eldor, L. Gepstein, High-resolution electrophysiological assessment of human embryonic stem cell-derived cardiomyocytes, Circ. Res. 91 (2002) 659–661.

[28] C. Mummery, D. Ward, C.E. van den Brink, Cardiomyocytes differentiation of mouse and human embryonic stem cells, J. Anat. 200 (2002) 489–493.

[29] D. Choi, H.J. Oh, U.J. Chang, S.K. Koo, J.X. Jiang, S.Y. Hwang, J.D. Lee, G.C. Yeoh, H.S. Shin, J.S. Lee, B. Oh, *In vitro* differentiation of mouse embryonic stem cells into hepatocytes, Cell Transplant. 11 (2002) 359–368.

[30] T. Yamada, M. Yoshikawa, S. Kanda, Y. Kato, Y. Nakajima, S. Ishizaka, Y. Tsunoda, *In vitro* differentiation of embryonic stem cells into hepatocytes-like cells identified by cellular uptake of indocyanine green, Stem Cells 20 (2002) 146–154.

[31] D.R. Newall, K.E. Beedles, The stem cell test: an *in vitro* assay for teratogenic potential. Results of a blind trial with 25 compounds, Toxicol. In Vitro 10 (1996) 229–240.

[32] G. Scholz, E. Genschow, I. Pohl, S. Bremer, M. Apparels, H. Rape, Prevalidation of the embryonic stem cell test EST—a new *in vitro* embryotoxicity test, Toxicol. In Vitro 13 (1999) 675–681.